Published for SISSA by Springer

Received: May 23, 2022
Accepted: June 26, 2022
Published: August 3, 2022

A database of Calabi-Yau orientifolds and the size of D3-tadpoles

Chiara Crinò,[a,b] **Fernando Quevedo,**[c] **Andreas Schachner**[c] **and Roberto Valandro**[a,b]

[a] *Dipartimento di Fisica, Universitá di Trieste, Strada Costiera 11, I-34151 Trieste, Italy*
[b] *INFN, Sezione di Trieste, via Valerio 2, I-34127 Trieste, Italy*
[c] *DAMTP, Centre for Mathematical Sciences, Wilberforce Road, Cambridge, CB3 0WA, U.K.*

E-mail: Chiara.Crino@ts.infn.it, fq201@damtp.cam.ac.uk, as2673@maths.cam.ac.uk, roberto.valandro@ts.infn.it

Abstract: The classification of 4D reflexive polytopes by Kreuzer and Skarke allows for a systematic construction of Calabi-Yau hypersurfaces as fine, regular, star triangulations (FRSTs). Until now, the vastness of this geometric landscape remains largely unexplored. In this paper, we construct Calabi-Yau orientifolds from holomorphic reflection involutions of such hypersurfaces with Hodge numbers $h^{1,1} \leq 12$. In particular, we compute orientifold configurations for all favourable FRSTs for $h^{1,1} \leq 7$, while randomly sampling triangulations for each pair of Hodge numbers up to $h^{1,1} = 12$. We find explicit string compactifications on these orientifolded Calabi-Yaus for which the D3-charge contribution coming from Op-planes grows linearly with the number of complex structure and Kähler moduli. We further consider non-local D7-tadpole cancellation through Whitney branes. We argue that this leads to a significant enhancement of the total D3-tadpole as compared to conventional SO(8) stacks with $(4+4)$ D7-branes on top of O7-planes. In particular, before turning-on worldvolume fluxes, we find that the largest D3-tadpole in this class occurs for Calabi-Yau threefolds with $(h^{1,1}_{+}, h^{1,2}_{-}) = (11, 491)$ with D3-brane charges $|Q_{\rm D3}| = 504$ for the local D7 case and $|Q_{\rm D3}| = 6,664$ for the non-local Whitney branes case, which appears to be large enough to cancel tadpoles and allow fluxes to stabilise all complex structure moduli. Our data is publicly available under the following link https://github.com/AndreasSchachner/CY_Orientifold_database.

Keywords: Flux Compactifications, String and Brane Phenomenology, Superstring Vacua, D-Branes

ArXiv ePrint: 2204.13115

Open Access, © The Authors.
Article funded by SCOAP[3].

https://doi.org/10.1007/JHEP08(2022)050

JHEP08(2022)050

Contents

1 Introduction **1**

2 From polytopes to Calabi-Yau hypersurfaces **3**
- 2.1 Triangulations of 4D reflexive polyhedra 3
- 2.2 Toric divisors and their topologies 4

3 Orientifold configurations **6**
- 3.1 Orientifold data 7
- 3.2 D7-branes 8
- 3.3 D-brane worldvolume flux 9
- 3.4 The D3-tadpole 10

4 Orientifold database **13**
- 4.1 An algorithm for finding orientifold configurations 13
- 4.2 Complete scan for CYs with $h^{1,1} \leq 7$ and random CYs at $h^{1,1} \leq 12$ 14
- 4.3 Hodge and Euler numbers of toric divisors 15
- 4.4 D3-charge in the database and non-local D7-tadpole cancellation 17

5 Example with $(h^{1,1}, h^{1,2}) = (11, 491)$ **24**

6 Conclusions **27**

A Examples with Whitney branes **28**
- A.1 Example with an SO(8) stack for a non-rigid SD1 divisor 28
- A.2 Example with a divisor with $h^{p,q} = h^{p,q}(K3)$ 30

B Simple example of CY with genus one fibrations: $\mathbb{P}[1, 1, 1, 6, 9]$ **31**

1 Introduction

Within the general context of flux compactifications in string theory, the goal of this paper is twofold: first, to discuss the size of D3-tadpoles in the presence of local and non-local D7 configurations. Secondly, to generate a database of Calabi-Yau (CY) orientifolds from reflection involutions that allows us to explicitly determine the size of D3-tadpoles in concrete models and that may have further applications.

Regarding the second goal, we provide a complete scan of type IIB orientifold models with O3/O7-planes for $h^{1,1} \leq 7$ for CY hypersurfaces obtained from the Kreuzer-Skarke (KS) database [1] via reflection involutions $z \to -z$ of toric coordinates. For $8 \leq h^{1,1} \leq 12$, we compute one triangulation per polytope to search for further appropriate models. We

JHEP08(2022)050

stress that our methods are easily applied to any triangulation of any polytope in the KS database.

The KS database [1] has received substantial attention in recent years, especially with the advent of software developments such as `CYTools` [2], making geometries at $h^{1,1} > 10$ readily accessible. Our investigation complements the analysis of [3, 4] for exchange involutions in the KS database for $h^{1,1} \leq 6$ as well as of [5] for Complete Intersection Calabi-Yaus (CICYs). Our database contains 71,941,643 orientifolds and extends previous orientifold databases of 2,004,513 CICY orientifolds [5] and 28,463 divisor exchange involutions [3].[1] The full data can be found in the following GitHub repository together with a `jupyter` notebook providing instructions on how to read and work with the data.

The size of the D3-tadpole is critical for stabilising moduli with fluxes [6, 7]. Recently, it has been argued that the required size of the D3-tadpole to stabilise all complex structure moduli with fluxes is $-Q_{\mathrm{D3}} > \alpha\, h^{1,2}$ [8] where $\alpha > 2/3$ in our convention.[2] This is known as the tadpole problem since it is challenging to obtain such large D3 charges in typical type IIB orientifold models [8, 9].[3]

The cancellation of D7 tadpoles also plays a role in determining the size of the maximum possible D3 charge, as D7-branes and O7-planes induce some D3-charge. Usually this is done locally in terms of stacks of D7-branes on top of O7 orientifold planes. However, there are other means to cancel the tadpoles. In particular the consideration of Whitney branes, that cancel non-locally the D7-charge of the O7-planes, since they are not localised on top of the O7 planes, allows the possibility of substantially enhancing the maximum value of the D3 charge needed to cancel the D3 tadpoles. We argue that construction with Whitney branes [11, 12] significantly surpass estimates for the D3-charge from SO(8) stacks of D7-branes on top of O7-planes. Similar observations have been made in [5] for general orientifolds of CICYs. Our models beat previous records for the total D3-charges obtained in type IIB setups as exemplified by table 1. Ultimately, the goal is to combine our investigation with de Sitter constructions which we will explore in an upcoming paper [13].

This paper is organised as follows. Next section is devoted to introductory material regarding the construction of CY orientifolds in terms of hypersurfaces of 4-dimensional reflexive polytopes. We describe the different types of toric divisors and their topological properties that are relevant for our subsequent discussions. In section 3 we discuss the orientifold involution and determine the different brane configurations needed to cancel the tadpoles induced by the O3 and O7 orientifold planes. In particular we point out the difference between local D7-branes and non-local D7 or Whitney branes and how they

[1] To be more concrete, we are working at the level of triangulations and not at the level of geometries. Hence, some triangulations may correspond to the same favourable Calabi-Yau geometry. In [3], the 28,463 triangulation-wise involutions reduced to 5,660 geometry-wise proper involutions out of which 4,482 are obtained from favourable geometries. In contrast, the CICY orientifolds of [5] are counted as distinct geometries. In this sense, the stated number of $\sim 7.2 \cdot 10^7$ should be taken with a grain of salt.

[2] In [8], $Q_{\mathrm{D3}} = \chi(Y_4)/24$, while in our convention $Q_{\mathrm{D3}} = -\chi(Y_4)/12$ as we compute the D3-charge in the perturbative type IIB double cover set up.

[3] As pointed out e.g. in [10], the tadpole conjecture could be phrased more precisely by stating that the landscape of vacua at large number of (complex structure) moduli may require singular geometries since the smoothness of the manifold was assumed to reach the conclusion.

JHEP08(2022)050

$\lvert Q_{\mathrm{D3}}\rvert$	Type	D7-tadpole cancellation	$h^{1,1}$	Reference
≤ 428	KS	non-local	3	[14]
≤ 72	CICY	local	≤ 19	[5]
≤ 264	CICY	non-local	≤ 19	[5]
≤ 272	CICY	local	4	[15]
≤ 60	KS	local	≤ 6	[3]
≤ 504	KS	local	≤ 12	our database
≤ 6664	KS	non-local	≤ 12	our database

Table 1. List of values for the total D3-charge contribution to the D3-tadpole.

contribute differently to the D3 tadpoles.

Section 4 describes in detail our database including the corresponding Hodge numbers and D3-brane charges, focusing on the general dependence of the D3 charges on the Hodge numbers and illustrating the maximum number of D3 charges that are relevant for the tadpole problem. First, we present a full scan for orientifold models for $h^{1,1} \leq 7$. Then we perform a random sampling for geometries with $8 \leq h^{1,1} \leq 12$ and identify the largest values of D3 charges for both local and non-local D7-brane configurations.

We describe the model with the largest D3-charge contribution in our database explicitly in section 5. We summarise our conclusions in section 6. In appendix A we provide concrete examples of Whitney branes analysing their factorisation property depending on the topology of the divisors. In a second appendix B, we present a simple example of a CY threefold with genus one fibration.

2 From polytopes to Calabi-Yau hypersurfaces

Here we collect some elementary definitions and formulae necessary for constructing CY hypersurfaces from 4-dimensional reflexive polytopes in the Kreuzer-Skarke (KS) database [1], see [16–18] for details of the construction.

2.1 Triangulations of 4D reflexive polyhedra

We construct CY threefolds as anti-canonical hypersurfaces in 4D Gorenstein toric Fano varieties [19]. To this end, we use combinatorial information encoded in 4-dimensional reflexive lattice polytopes. A complete list of 4D reflexive polytopes was initiated by Kreuzer and Skarke [1]. A database of CY threefolds with $h^{1,1} \leq 6$ was generated in [3, 16, 20], while [2, 18, 21, 22] explored regimes up to $h^{1,1} = 491$ and their phenomenological implications in [23, 24].

JHEP08(2022)050

To construct CY threefolds, one begins with two reflexive polytopes Δ and Δ° based on two 4D lattices $M \cong \mathbb{Z}^4$ and $N \cong \mathbb{Z}^4$ with a pairing $\langle \cdot\,, \cdot \rangle$ so that $\Delta \in M_\mathbb{R} = M \otimes \mathbb{R}$ and $\Delta^\circ \in N_\mathbb{R} = N \otimes \mathbb{R}$ satisfy

$$\langle \Delta, \Delta^\circ \rangle \geq -1\,. \tag{2.1}$$

We associate to the polytope Δ° a fan Σ in the following way. Reflexivity of Δ° implies that the origin of N is the unique interior lattice point of Δ°. We denote all other lattice points of Δ° by ν_i. The latter correspond to primitive generators of the rays of the fan Σ. The cones of Σ are given by a triangulation of Δ°, i.e., special subsets of the ν_i with each containing the generators of a cone. We will focus on so-called *fine, regular, star triangulations*[4] (FRSTs), whose fan describes a simplicial toric 4-fold denoted $\mathbb{P}_\Sigma$. One can introduce weighted, homogeneous coordinates z_i on $\mathbb{P}_\Sigma$. Within $\mathbb{P}_\Sigma$, the CY threefold X is found as the zero locus of a polynomial $P = \sum_m c_m\, p_m$, where p_m are monomials in z_i's and c_m are coefficients related to the complex structure moduli of X. The individual monomials p_m appearing in P are encoded by Δ, also called the *Newton polytope* of the hypersurface. They are easily computed from (see e.g. eq. (A.8) in [16])

$$p_m = \prod_i z_i^{\langle m, \nu_i \rangle + 1}\,, \quad m \in \Delta \cap M\,. \tag{2.2}$$

Although $\mathbb{P}_\Sigma$ does not need to be smooth, every FRST leads to a smooth hypersurface X [19]. We focus exclusively on *favourable* geometries where

$$h^{1,1}(X) = \dim(\mathrm{Pic}(\mathbb{P}_\Sigma))\,, \tag{2.3}$$

that is, the Kähler moduli on X descend from those of the ambient space $\mathbb{P}_\Sigma$.

Computationally, it is generically expensive to compute all triangulations for a given Δ°. For sufficiently simple polytopes, that is, those with few lattice points, all triangulations were obtained in [16] up to $h^{1,1}(X) = 6$. Here, only a small subset of the triangulation data was required to define the geometry of X. Specifically, everything happening inside faces of co-dimension one can be ignored. In our scan, we check all favourable geometries for $h^{1,1}(X) \leq 7$ and provide partial results up to $h^{1,1}(X) = 12$.

2.2 Toric divisors and their topologies

Each weighted, homogeneous coordinate z_i of $\mathbb{P}_\Sigma$ corresponds to a point on the boundary of Δ°. The loci $\tilde{D}_i = \{z_i = 0\}$ are called *prime toric divisors* (see e.g. [18] for details). The subset of such divisors which intersect X transversely corresponds to points that lie in faces of Δ° of dimension ≤ 2. Intersecting such a locus with the CY hypersurface equation, one gets a divisor $D_i \in H^{1,1}(X, \mathbb{Z})$ which defines a 4-cycle in X dual to a 2-cycle ω_i. Since we focus exclusively on favourable polytopes and geometries, all such prime toric divisors are irreducible on X. Hence, $H_4(X, \mathbb{Z})$ is generated by any basis constructed from $\{D_i\}$, $i = 1, \ldots, h^{1,1}(X) + 4$.

[4] A triangulation is *fine* if all points not interior to facets appear as vertices of a simplex. Further, it is *star* if the origin is a vertex of each full-dimensional simplex. *Regularity* implies that Σ is the normal fan of a polytope and essentially ensures that $\mathbb{P}_\Sigma$ and X are projective, see [25].

JHEP08(2022)050

The Hodge numbers of divisors are collectively denoted as

$$h^{\bullet}(D) = \left\{h^{0,0}(D), h^{0,1}(D), h^{0,2}(D), h^{1,1}(D)\right\} . \tag{2.4}$$

A rigid divisor D_{rig} is defined as

$$h^{\bullet}(D_{\text{rig}}) = \left\{1, 0, 0, h^{1,1}(D_{\text{rig}})\right\} . \tag{2.5}$$

Prototypical examples include del Pezzo divisors dP_n, $n = 0, \ldots, 8$ (where $\text{dP}_0 = \mathbb{P}^2$) and the Hirzebruch surface $\mathbb{F}_0 = \mathbb{P}^1 \times \mathbb{P}^1$, for which $h^{(1,1)}(D_{\text{dP}_n}) = n + 1$ and $h^{(1,1)}(D_{\mathbb{F}_0}) = 2$. These divisors play a special role since they can be shrunk to a point allowing for SM realisations on D3-branes placed at the tip of the singularity [15]. Rigid divisors with $h^{(1,1)}(D) > 9$ are typically referred to as *non-shrinkable*.

For later purposes, we distinguish other common types of divisors as follows, see also [3]:

1. Wilson divisors: $h^{\bullet}(D) = \{1, h^{1,0}, 0, h^{1,1}\}$ with both $h^{1,0} \neq 0$ and $h^{1,1} \neq 0$,
2. K3 divisor: $h^{\bullet}(D) = \{1, 0, 1, 20\}$,
3. SD1: $h^{\bullet}(D) = \{1, 0, 1, 21\}$,
4. SD2: $h^{\bullet}(D) = \{1, 0, 2, 30\}$.

To compute these Hodge numbers, we follow the steps outlined in [17, 26], that we now review.[5] As said above, each toric divisor $D_i \in H^{1,1}(X, \mathbb{Z})$ is associated with a lattice point ν_i on Δ°. Its Hodge numbers $h^{0,p}$ can be obtained from the location of ν_i inside Δ°. In fact, one finds the following [19, 29]:

1. *Rigid divisors:* a toric divisor D_i is rigid if

$$\ell^*(\Theta) = 0 , \tag{2.6}$$

   where ℓ^* is the sum of all interior points of the face Θ, which is the dual of the face containing ν_i.

2. *Deformation divisors:* divisors with $h^{0,2}(D_i) > 0$ and $h^{0,1}(D_i) = 0$ are associated with points ν_i corresponding to vertices of Δ° so that

$$h^{0,1}(D_i) = 0 , \qquad h^{0,2}(D_i) = \ell^*\left(\Theta^{[3]}\right) , \tag{2.7}$$

   in terms of the dual face $\Theta^{[3]}$ to $\nu_i = \Theta^{\circ[0]}$.

3. *Wilson divisors:* lastly, divisors D_i associated with points ν_i inside a one-dimensional face $\Theta^{\circ[1]}$ of Δ° give rise to

$$h^{0,1}(D_i) = \ell^*\left(\Theta^{[2]}\right) , \qquad h^{0,2}(D_i) = 0 , \tag{2.8}$$

   in terms of the dual face $\Theta^{[2]}$ to $\Theta^{\circ[1]}$.

[5] Another way to computing divisor topologies uses the `cohomCalg` package [27, 28] which is however limited when applied to models with $h^{1,1}(X) \geq 6$. In particular, the authors of [3] computed the Hodge numbers of divisors up to $h^{1,1}(X) = 6$ in this way.

JHEP08(2022)050

The above conditions can easily be checked using Sage [30]. The remaining Hodge numbers can then be inferred from the Euler characteristic and the arithmetic genus

$$\chi(D) = 2h^{0,0} - 4h^{0,1} + 2h^{0,2} + h^{1,1} = \int_D c_2(D)\,, \tag{2.9}$$

$$\chi_0(D) = h^{0,0} - h^{0,1} + h^{0,2} = \frac{1}{12}\int_D \Big(c_1(D)^2 + c_2(D)\Big)\,. \tag{2.10}$$

The r.h.s. can be easily computed from the CY data, by using adjunction formula $c_2(X) = c_2(D) - c_1(D)^2$ and $c_1(D) = -\iota^* D$ for a CY:

$$\int_D c_2(D) = \int_D (D^2 + c_2(X))\,, \quad \int_D \Big(c_1(D)^2 + c_2(D)\Big) = \int_D (2D^2 + c_2(X))\,. \tag{2.11}$$

The above can be solved for $h^{0,0}$ and $h^{1,1}$ as

$$h^{0,0} = \chi_0(D) + h^{0,1} - h^{0,2}\,, \qquad h^{1,1} = \chi(D) - 2\chi_0(D) + 2h^{0,1}\,. \tag{2.12}$$

Instead of computing Hodge numbers explicitly, it can also be useful to check the sufficient conditions for del Pezzo divisors using their intersection numbers. Indeed, a del Pezzo divisor must satisfy the following topological conditions

$$\int_X D_s^3 = k_{sss} = 9 - n > 0\,, \qquad \int_X D_s^2\, D_i \leq 0 \qquad \forall\, i \neq s\,. \tag{2.13}$$

We moreover look for divisors D_s that satisfy the following *diagonality* condition [31]

$$k_{sss}\; k_{sij} = k_{ssi}\; k_{ssj} \qquad\qquad \forall\;\; i,j\,. \tag{2.14}$$

If this condition is satisfied, then the volume of the associated 4-cycle D_s is a complete-square:

$$\tau_s = \frac{1}{2}\, k_{sij} t^i\, t^j = \frac{1}{2\, k_{sss}}\, k_{ssi}\, k_{ssj} t^i\, t^j = \frac{1}{2\, k_{sss}}\, \Big(k_{ssi}\, t^i\Big)^2\,, \tag{2.15}$$

where we sum over i, j but not over s. This condition is commonly used in the LVS [32, 33] by ensuring that the volume form is of swiss cheese type. Furthermore, it allows to generate del Pezzo singularities by shrinking the divisor to a point along one direction of the Kähler moduli space which is heavily utilised in constructions of branes at singularities, see [15] for a recent discussion and further references.

3 Orientifold configurations

We focus on involutions of toric coordinates of the form $\sigma_k : z_k \to -z_k$ for which $h^{1,1}_- = 0$ (if the corresponding geometry is favourable, see e.g. [3] for a discussion). For each involution, we obtain configurations of Op-planes given by fixed point loci of the associated involution σ_k. Tadpole and anomaly cancellation is ensured by adding an appropriate D-brane setup.

JHEP08(2022)050

3.1 Orientifold data

We consider involutions with O3/O7 orientifold planes. An O7-plane wraps a fixed surface D_i in the CY three-fold, while an O3-plane is at an isolated fixed point of the involution.

An important topological invariant that we will need later to compute the D3-charge contributions is the Euler characteristic (2.9) of a (smooth) divisors D_i. As said above, it is given by the integral $\int_{D_i} c_2(D_i)$ which is computed from the topological data

$$\chi(D_i) = k_{iii} + \int_{D_i} c_2(X) \tag{3.1}$$

$$= 2h^{0,0}(D_i) - 4h^{1,0}(D_i) + 2h^{2,0}(D_i) + h^{1,1}(D_i)\,. \tag{3.2}$$

The knowledge of the topology of the fixed point set allows to compute other integers invariants of the CY orientifold. In particular the cohomology groups $H^{p,q}(X)$ split into even and odd subspaces of the (pull-back of the) orientifold involution. Their dimensions are called $h^{p,1}_+(X)$ and $h^{p,1}_-(X)$ respectively. To compute them, we use Lefschetz fixed point theorem which states that

$$\sum_i (-1)^i (b^i_+(X) - b^i_-(X)) = \chi(O_\sigma)\,, \quad b^i_\pm(X) = \sum_{p+q=i} h^{p,q}_\pm(X) \tag{3.3}$$

in terms of the even/odd Betti numbers $b^i_\pm(X)$. Here, we will have

$$\chi(O_\sigma) = \sum_i \chi(O7_i) + \sum_k \chi(O3_k)\,, \qquad \text{with } \chi(O3_k) = 1\,. \tag{3.4}$$

For CY threefolds, the expression (3.3) simplifies to

$$2 + 2\left(h^{1,1}_+(X) - h^{1,1}_-(X)\right) - 2\left(h^{1,2}_+(X) - h^{1,2}_-(X) - 1\right) = \chi(O_\sigma)\,. \tag{3.5}$$

Since we know $h^{1,1}_\pm(X)$ (in cases under study $h^{1,1}_-(X) = 0$ and $h^{1,1}_+(X) = h^{1,1}(X)$), we can use this relation to obtain the Hodge numbers $h^{1,2}_\pm(X)$. We need to solve the equations:

$$h^{1,2}_+(X) + h^{1,2}_-(X) = h^{1,2}(X)\,, \qquad h^{1,2}_+(X) - h^{1,2}_-(X) = h^{1,1}(X) + 2 - \frac{\chi(O_\sigma)}{2}\,. \tag{3.6}$$

Below, we use this data to discard models where the computation of $h^{1,2}_\pm(X)$ lead to non-integer values, as this is a signal of possible unwanted singularities.

To detect more subtle singularities which are not manifest in the orientifold data, we look at the underlying polytopes. Let us just reiterate again that we are interested in involutions of a single homogeneous toric coordinate $z_k \to -z_k$ which is associated with one of the boundary lattice points ν_k of Δ° not interior to facets (i.e., 3-faces). Recalling (2.2), the invariant CY equation for $z_k \to -z_k$ is obtained from the monomials

$$p^{(k)}_m = \prod_i z_i^{\langle m,\nu_i\rangle + 1}\,, \quad m \in \Delta_k \cap M \tag{3.7}$$

where we define

$$\Delta_k = \{m \in \Delta \,:\, \langle m, \nu_k\rangle + 1 \in 2\mathbb{N}\}\,. \tag{3.8}$$

JHEP08(2022)050

We argue that the properties of Δ_k are in one-to-one correspondence with the hypersurface obtained from tuning the CY equation to be invariant under $z_k \to -z_k$.

Removing (the non-invariant) monomials for the CY defining equation can force some singularities: either 1) the hypersurface is forced to touch singularities of the ambient space, or 2) the defining polynomial describes now a singular hypersurface (there are points where the differential of the equation and the equation itself vanish simultaneously). Since we want to work with smooth spaces, we need to discard models where the involution forces singularities.

The desired invariant CY X can be obtained from triangulations of the polar dual Δ_k°. Since we are interested in collecting big numbers, we decide to keep in the analysis only invariant CY's corresponding to favorable Δ_k° and reflexive Δ_k. For these CY we can claim smoothness. We checked in several models that the excluded CY's were actually singular.[6]

3.2 D7-branes

In order to cancel the D7-tadpole induced by the O7-planes, we add D7-branes on the appropriate divisors.

The D7-charge of an O7-plane wrapping the divisor D_i is $-8[D_i]$. The easiest way to cancel the D7-tadpole is then to put 4 D7-branes plus their 4 images on top of the O7-plane. The D7-brane configuration is given in this case by $z_i^8 = 0$. The gauge group supported on such a stack is SO(8).

The other extreme case is to cancel the D7-tadpole by a fully recombined D7-brane in the homology class $8[D_i]$. This is called *Whitney brane*, as it is forced to have a singular worldvolume of the form of the Whitney umbrella [11, 12, 34]:

$$\eta^2 - z_i^2 \chi = 0\,, \tag{3.9}$$

where $z_i \in \mathcal{O}(D_i)$, $\eta \in \mathcal{O}(4D_i)$ and $\chi \in \mathcal{O}(6D_i)$. The sections η and χ are invariant under the orientifold involution, while $z_i \mapsto -z_i$. This brane supports no continuous gauge group and has zero chiral intersection with (fluxless) D7- or E3-branes supported on an intersecting divisor [12].

For a generic toric divisor with high weights, the locus (3.9) is connected. However, there can be particular cases when the generic sections η, χ of the line bundles $\mathcal{O}(4D_i), \mathcal{O}(6D_i)$ factorise. For instance, it may happen that

$$\eta = z_j^m \eta'\,, \quad \chi = z_j^{2m} \chi'\,. \tag{3.10}$$

Then the equation of the configuration will be

$$z_j^{2m} \left(\eta'^2 - z_i^2 \chi' \right) = 0\,. \tag{3.11}$$

If this happens, we recover a stack of D7-branes on $z_j = 0$ plus a Whitney brane of lower degree in the homology class $8[D_i] - 2m[D_j]$ (see e.g. [14]).

[6] Of course, string theory is well defined also on singular spaces. In the database we provide on GitHub, the reader can find also the data of the singular models. However we decide to stay on the safe side, studying models with smooth geometry where the usual formulae to compute topological invariants work well.

JHEP08(2022)050

A particular important example of a factorisation like (3.10) appears when D_i is a *rigid divisor*. In this case $\eta \propto z_i^4$ and $\chi \propto z_i^6$ and we are left with a configuration, whose locus is $z_i^8 = 0$, i.e. we have four D7-branes plus their four images on top of the O7-plane, generating an SO(8) D7-brane stack.

Also special non-rigid divisors can lead to a factorisation of the Whitney brane. In fact, whenever D_i is a K3 surface the Whitney brane splits into a $\mathrm{U}(1)^4$ configuration with four D7-branes plus their four images. In our analysis we found that this kind of factorization often happens for divisors with $h^{2,0} = 1$. We provide two explicit examples in appendix A.

3.3 D-brane worldvolume flux

Let us assume that the orientifold model contains stacks of E3/D7-branes wrapped on a divisors D. We can then turn on a gauge flux

$$\mathcal{F} = F_2 - \iota^* B_2 \,, \tag{3.12}$$

where F_2 is the field strength of the worldvolume U(1) gauge theory, B_2 is the NSNS 2-form potential and $\iota^* : H^2(X) \to H^2(D)$ is the pull-back map on D.

Freed-Witten anomaly cancellation [35] requires the following quantization condition on F_2:

$$F_2 + \frac{c_1(D)}{2} \in H^2(D, \mathbb{Z}) \,, \tag{3.13}$$

where $c_1(D) = -\iota^* D$ for X a CY. This implies that the following expression for $\mathcal{F}$ fulfills this condition:

$$\mathcal{F} = \sum_{k=1}^{h^{1,1}(X)} n_k \, \iota^* D_k + \frac{1}{2} \iota^* D - \iota^* B_2 \qquad \text{with} \qquad n_k \in \mathbb{Z} \tag{3.14}$$

and with $\{D_k\}$ an integral basis of $H^2(X, \mathbb{Z})$.

If D is wrapped by an O(1) ED3-instanton, then the orientifold invariance of the configuration requires

$$\mathcal{F}_{\mathrm{ED3}} = 0 \,. \tag{3.15}$$

This can be achieved by properly choosing the background of B_2, i.e. s.t.

$$\iota^* B_2 = \iota^* D_{\mathbb{Z}} - \frac{1}{2} \iota^* D \qquad \text{with } \; D_{\mathbb{Z}} \in H^2(X, \mathbb{Z}) \,. \tag{3.16}$$

Rank-2 E3 instantons with a non-trivial gauge bundle can also be allowed by a B_2 that does not fulfill (3.16) [36].

Let us come to the Whitney brane (3.9) in the homology class $8[D_i]$. The Whitney brane can support an integral flux, that as we will see contribute to the D3-charge. When this flux is present, the defining polynomial χ is forced to take the form $\chi = \psi^2 - \rho\tau$ with $\psi \in \mathcal{O}(3D_i)$, $\rho \in \mathcal{O}(3D_i - 2F + 2B_2)$ and $\tau \in \mathcal{O}(3D_i + 2F - 2B_2)$, where $F \in H^2(X, \mathbb{Z})$ and B_2 is the B-field [11]. The flux data is encoded in the choice of the line bundles

$$\mathcal{O}(3D_i - 2F + 2B_2) \qquad \text{and} \qquad \mathcal{O}(3D_i + 2F - 2B_2), \tag{3.17}$$

JHEP08(2022)050

i.e. in the choice of the integral two-form F. One gets a zero flux when one of these line bundles is trivial. Notice that this can be achieved when $D_i + 2B$ is an even form (remember that B can take half-integral values), that may not happen.

When one of the line bundles in (3.17) has no holomorphic sections, then either ρ or τ is forced to vanish. In this case, the Whitney brane locus factorizes as

$$(\eta + z_i\psi)(\eta - z_i\psi) = 0\,, \tag{3.18}$$

i.e. it splits into a pair of one D7-brane and its orientifold image, both in the homology class $[4D_i]$. Hence, in order for the Whitney brane to be non-factorised one requires that the line bundles (3.17) have holomorphic sections, i.e.

$$-\frac{3D_i}{2} + B_2 \leq F \leq \frac{3D_i}{2} + B_2\,. \tag{3.19}$$

Even when the condition (3.19) holds, one can set $\rho = \tau = 0$ by a deformation of the Whitney brane. Correspondingly, the Whitney branes splits as in (3.18). The U(1) D7-brane has then a flux $\mathcal{F} = \iota^*(F - B_2)$, where F is the same two-form appearing in (3.17). When this happens, the D7-brane can have chiral intersections with some E3-instantons. This will be counted by the formula

$$0 = \int_{\mathrm{D7}\cap\mathrm{ED3}} (\mathcal{F}_{\mathrm{D7}} - \mathcal{F}_{\mathrm{ED3}}) = D_{\mathrm{D7}} \cdot D_{\mathrm{ED3}} \cdot \mathcal{F}_{\mathrm{D7}}\,. \tag{3.20}$$

A non-perturbative instanton contribution to the 4D superpotential requires the absence of chiral modes (for non-chiral modes, see footnote 21 in [15]) at the intersection of D7-branes and ED3-instantons. This generally limits the flux allowed on the D7-branes.

A U(1) D7-brane with fluxes supports a generically non-zero FI-term:

$$\xi_{\mathrm{D7}} = \frac{1}{4\pi\mathcal{V}} \int_{D_i} \mathcal{F}_{\mathrm{D7}} \wedge J\,. \tag{3.21}$$

This term, if non-zero, requires a non-vanishing VEV for scalar modes at the intersection between D7 and its image in order to cancel the D-term potential.[7] If F satisfies (3.19), this corresponds to deforming the branes switching on non-zero ρ and τ; this recombines the two branes into a Whitney brane. If the condition (3.19) is not fulfilled, then only ρ or τ can be non-zero and we generate a T-brane background, i.e. the two branes form a bound state whose locus is still (3.18) [37].

3.4 The D3-tadpole

We now compute the induced D3-charge from the orientifold configuration. Generally, the D3-tadpole cancellation condition reads

$$N_{\mathrm{D3}} + N_{\mathrm{D3'}} + N_{\mathrm{flux}} = -Q_{\mathrm{D3}}\,, \qquad \text{with } Q_{\mathrm{D3}} = Q_{\mathrm{D7}}^{\mathrm{tot}} + Q_{Op}^{\mathrm{tot}}\,, \tag{3.22}$$

[7] There is also the possibility that the sign of ξ generates a D-term that is strictly positive; in this case this leads to SUSY breaking [37].

JHEP08(2022)050

where

$$Q^{\rm tot}_{\rm D7} = \sum_i \left(Q^i_{\rm D7} + Q^i_{D7'}\right)\,, \quad Q^{\rm tot}_{Op} = \sum_k Q^k_{\rm O3} + \sum_l Q^l_{\rm O7}\,. \tag{3.23}$$

For O7/O3-planes, we collect

$$Q^i_{\rm O7} = -\frac{\chi(D_i)}{6}\,, \quad Q^i_{\rm O3} = -\frac{1}{2}\,, \tag{3.24}$$

whereas a U(1) D7-brane contributes as

$$Q^i_{\rm D7} = -\frac{\chi(D_i)}{24} - \frac{1}{2}\int_{D_i} \mathcal{F}\wedge\mathcal{F}\,. \tag{3.25}$$

For later convenience, we refer to $Q^{\rm tot}_{\rm SO(8)}$ and $Q^{\rm tot}_{\rm WD7}$ as the D3-charge contribution coming from rigid D7-branes and Whitney branes respectively. The first one is easy to compute: when all the four D7 branes have the same flux $\mathcal{F}$, then the group is broken to SU(4) (the diagonal U(1) get a Stückelberg mass due to Green-Schwartz mechanism) and the contribution of the stack to the D3-tadpole is

$$Q^{\rm tot}_{\rm SO(8)} = 8Q_{\rm one\,D7} = -\frac{\chi(D_i)}{3} - 4\int_{D_i} \mathcal{F}\wedge\mathcal{F}\,. \tag{3.26}$$

For the Whitney brane the situation is a bit different. The expression of its total D3-charge can be derived in a simple way [12]: the D3-charge does not change under recombination or splitting of branes; hence we can compute it in the phase where the Whitney brane splits into a U(1) brane and its image. Hence, for a Whitney brane in the class $8D_i$

$$Q^i_{WD7} = -\frac{\chi(4D_i)}{12} - \int_X D_i\wedge(F-B_2)\wedge(F-B_2)\,. \tag{3.27}$$

with F given in (3.19). The geometric contribution of the Whitney brane is different from the geometric contribution of the brane/image-brane system [11]. In fact, the D3-charge contributions from geometry and from the flux encoded into the line bundles (3.17) are [11, 38]

$$Q^i_{WD7,\rm geom} = -\frac{1}{3}\int_X D_i\wedge(43D_i\wedge D_i + c_2(X)) = -\frac{\chi(4D_i)}{12} - 9\int_X D_i^3\,, \tag{3.28}$$

$$Q^i_{WD7,\rm flux} = \int_X D_i\wedge(3D_i - 2F + 2B_2)\wedge(3D_i + 2F - 2B_2)\,. \tag{3.29}$$

One can easily check that the sum of the two gives (3.27) and that $Q^i_{WD7,\rm flux}$ is identically zero when the line bundles (3.17) are trivial. If $D_i + 2B_2$ is an even integral form, one can actually take zero flux and make $Q^i_{WD7,\rm flux}$ vanish.[8] Generically this is not possible, but it is always possible to choose F such that $Q^i_{WD7,\rm flux} \ll Q^i_{WD7,\rm geom}$. This will justify, in our analysis, to approximate the D3-charge of a Whitney brane by its geometric contribution.

[8] Actually, it is enough that $\iota^*_{D_i}(3D_i + 2B_2 - 2F)$ vanishes, in order to have $Q^i_{WD7,\rm flux} = 0$.

JHEP08(2022)050

Before we continue, let us make a few estimates on the D3-charge contributions. Let us start from

$$-Q_{\rm O7}^{\rm tot} = \sum_i \frac{\chi(D_i)}{6} = \frac{\chi(O_\sigma) - N_{\rm O3}}{6} = \frac{h^{1,1}(X) + h_-^{1,2}(X) - h_+^{1,2}(X) + 2}{3} - \frac{N_{\rm O3}}{6}\,,$$

where we used (3.4) and (3.5) (with $h_-^{1,1}(X) = 0$) and where $N_{\rm O3}$ is the number of isolated fixed points in X. We conclude that there are two possibilities of increasing this value by investigating models with either many Kähler or instead many complex structure moduli. We are going to observe this scaling with respect to $h_-^{1,2}$ quite frequently below for orientifolds with $h_+^{1,2} = 0$, see in particular figure 3.

Now, assume we have O7-planes on divisors D_i and that we cancel their D7-charge by putting 4 D7-branes plus their 4 images in each D_i (producing a bunch of SO(8) stacks). This is the choice that minimize the D3-charge contribution from O7/D7's. Let us now consider several CY's X and involutions and let us estimate what is the maximum that we can get for the D3-charge for this minimal configuration, where we cancel the D7-tadpole locally (i.e. with only SO(8) stacks). One may use (3.26) and write (in the absence of worldvolume fluxes)

$$-Q_{\rm SO(8)}^{\rm tot} = \sum_i \frac{\chi(D_i)}{3} = 2\frac{h^{1,1}(X) + h_-^{1,2}(X) - h_+^{1,2}(X) + 2}{3} - \frac{N_{\rm O3}}{3} \tag{3.30}$$

to arrive at [5, 8, 10, 11]

$$-Q_{\rm D3} = -Q_{\rm O3}^{\rm tot} - Q_{\rm O7}^{\rm tot} - Q_{\rm SO(8)}^{\rm tot} \leq 2 + h^{1,1} + h^{1,2}\,, \tag{3.31}$$

where in the last step we used $Q_{\rm O3}^{\rm tot} = -\frac{N_{\rm O3}}{2}$ and the fact that $h_-^{1,2}(X) - h_+^{1,2}(X) \leq h^{1,2}(X)$.

In the KS database, this implies $-Q_{\rm D3} \leq 504$ for e.g. CYs with Hodge numbers $(h^{1,1}, h^{1,2}) = (11, 491)$ which we discuss further below.

D3-tadpole in F-theory. A perturbative type IIB orientifold compactification can always be described in F-theory language. The F-theory compactification manifold is a CY fourfold that is an elliptic fibration over the base space $B_3 = X/\sigma$, that is the quotient of X by the orientifold involution. If the involution allows to cancel all the D7-tadpoles by Whitney branes, this corresponds to a smooth CY fourfold in F-theory. Splitting the Whitney branes in type IIB, producing a non-trivial gauge group G, corresponds to deforming the fourfold generating codimension-3 (abelian G) or codimension-2 (non-abelian G) singularities. If the fixed point locus includes a rigid divisor, then the D7-branes on that divisor support an SO(8) gauge group that cannot be deformed; this corresponds to a so called non-Higgsable cluster in the F-theory fourfold [39, 40], i.e. in this case a non-deformable D_4 singularity.

The D3-tadpole cancellation condition in F-theory takes the form:[9]

$$\frac{1}{2}\int_{Y_4} G_4 \wedge G_4 + N_{\rm D3} = \frac{\chi(Y_4)}{24}\,, \tag{3.32}$$

[9] We note that $\chi(Y_4)/24 = -Q_{\rm D3}/2$ when compared to D3-tadpole in (3.22) given that we work with the double cover in section 3.4.

JHEP08(2022)050

where[10] $\chi(Y_4) = 6\left(8 + h^{1,1}(Y_4) + h^{1,3}(Y_4) - h^{1,2}(Y_4)\right)$ is the Euler characteristic of the fourfold. When the fourfold is singular, this formula still applies, provided one uses the resolved fourfold [11, 38, 41]. However, the geometric contribution to the tadpole decreases as one makes a deformation from a smooth to a singular fourfold (with some gauge group and matter). This is consistent with what one observes in type IIB: splitting the Whitney brane, the D3 contribution decreases (in absolute value) [11].

The large D3-charges that are usually mentioned in literature as coming from F-theory backgrounds, correspond typically to smooth fourfold (with no gauge group or matter). These large D3-charges can be reached in type IIB by canceling the D7-tadpole by means of Whitney branes.

4 Orientifold database

In this section, we generate a database of CY orientifolds models based on the general information summarised in section 3. An essential tool in this context is the `CYTools` package [2] which allows us to construct FRSTs from polytopes at arbitrary $h^{1,1}$. Beyond that, we implemented a basic algorithm to construct CY orientifolds from the polytope and triangulation data from reflection involutions. We test this implementation up to $h^{1,1} = 12$. As an application of our database, we investigate the size of D3-charge contributions.

4.1 An algorithm for finding orientifold configurations

For each CY X and each choice of involution, we determine the fixed point set in the following way.

1. We first find the CY equation that is symmetric under the chosen involution, by determining the set of invariant monomials under σ_k (keeping only those in (2.2) involving even powers of z_k).

2. We determine loci of points of the toric ambient fourfold $\mathbb{P}_\Sigma$ that are fixed under σ_k: in practice, we consider the action on the coordinates z_j of σ_k and $\sigma_k \cdot \zeta_a$, with ζ_a the $\mathbb{C}^*$ toric equivalences, and taking into account the SR ideal.

3. We check whether the invariant CY equation vanishes at a given locus. If no, a complex co-dimension n locus in $\mathbb{P}_\Sigma$ determines the presence of an Om-plane with $m = 3 + 2(3 - n)$. If yes, a co-dimension n locus corresponds to an Om-plane with $m = 3 + 2(4 - n)$.

We consider involutions that generate O3- and O7-planes, so in our scan there are no O5/O9-planes which can however arise for exchange involutions [3].

The number of O3-planes is determined from the intersection numbers either in the CY for co-dimension 3 or in the ambient fourfold for co-dimension 4 fixed point loci. The latter can be obtained from `CYTools` where we take special care of singularities in the ambient space.

[10] This is obtained from $\chi(Y_4) = 4+2h^{1,1}-4h^{1,2}+2h^{1,3}+h^{2,2}$ together with $h^{2,2} = 44+4h^{1,1}-2h^{1,2}+4h^{1,3}$.

JHEP08(2022)050

$h^{1,1}$	2	3	4	5	6	7	total
polytopes	36	244	1,197	4,990	17,101	50,376	73,944
fav. polytopes	36	243	1,185	4,897	16,608	48,221	71,190
fav. FRSTs	48	525	5,330	56,714	584,281	5,990,333	6,637,231
involutions	184	3,035	39,653	495,854	5,777,640	65,625,277	71,941,643
smooth invol.	138	1,975	22,933	230,886	2,081,080	17,875,122[11]	20,212,134
only O7	49	598	3,896	25,391	177,468	1,336,960	1,544,362
≥ 2 coin. O3	71	1,089	15,497	164,634	1,480,968	12,596,558	14,258,817

Table 2. Number of CY orientifolds obtained in our scan. We also collected the numbers of the models with only O7-planes or more than one coincident O3-plane.

A similar algorithm to determine the O-plane configurations in the context of exchange involutions was introduced in [3]. In this sense, our work provides a complementary analysis for the geometries with $h^{1,1} \leq 6$, while providing additional statistics up to $h^{1,1} = 12$. What sets our database apart is the study of Whitney brane configurations as opposed to simple SO(8) stacks of D7-branes.

4.2 Complete scan for CYs with $h^{1,1} \leq 7$ and random CYs at $h^{1,1} \leq 12$

The database we produce consists of two sets of data:

1. We compute *all* FRSTs of *all* favourable polytopes at $h^{1,1} \leq 7$. For each toric coordinate z_k, we construct the orientifold configuration associated with the involution $z_k \to -z_k$. This data is summarised in table 2.

2. For each combination of Hodge numbers $(h^{1,1}, h^{1,2})$ up to $h^{1,1} = 12$, we generate up to 20 *random* FRSTs of ≤ 20 favourable polytopes. Again, we build orientifolds for involutions of each toric coordinate $z_k \to -z_k$. The results are given in table 3.

The full data are collected in a GitHub repository which can be found here: https://github.com/AndreasSchachner/CY_Orientifold_database.

As we said, for each triangulation, we analyse each involution $z_k \mapsto -z_k$ and determine the fixed point set. In table 2 and in table 3 we report the numbers of independent[12] involutions. Some of these involutions lead to singularities in the CY threefold. As explained

[11] Parts of the orientifold data for $h^{1,1} = 7$ are still work in progress and will be updated in the repository as soon as possible.

[12] We count the number of inequivalent involutions given that inverting coordinates with the same weight vector gives rise to equivalent involutions up to coordinate redefinitions.

JHEP08(2022)050

$h^{1,1}$	7	8	9	10	11	12	total
fav. polytopes	1,219	1,498	1,587	1,555	1,623	1,807	8,980
fav. FRSTs	4,560	6,897	9,968	12,189	15,748	15,430	64,792
involutions	49,326	81,911	128,403	169,775	235,216	245,989	910,620
smooth invol.	6,491	9,102	13,041	15,713	21,892	24,154	90,393
only O7	1,769	2,608	3,493	3,543	4,330	4,772	20,515
≥ 2 coin. O3	3,168	4,084	5,865	6,692	9,978	9,507	39,294

Table 3. Random FRSTs for favourable polytopes between $7 \leq h^{1,1} \leq 12$. We selected up to 20 polytopes for each combination of Hodge numbers $(h^{1,1}, h^{1,2})$ available in the KS database.

at the end of section 3.1, we can detect the singular models. We refer to models that do not present manifest pathologies as *smooth involutions*.

We finally report the number of models that contain only O7-planes and those that contain at least two O3 planes that can collide by a complex structure deformation of the threefold. Models in both classes will be suitable for T-brane de Sitter uplift, while models in the last class are needed in order to implement de Sitter uplift by an anti-D3-brane at the tip of a highly warped throat realising the scenario outlined in [42–44].

As observed in [15], there is a trend that del Pezzo divisors dP_n with $1 \leq n \leq 5$ embedded into CY threefolds obtained from the KS database never satisfy the diagonality condition (2.14), cf. table 4. Our analysis extends the conjecture of [15] to all FRSTs at $h^{1,1} = 6, 7$.

4.3 Hodge and Euler numbers of toric divisors

In this section, we investigate the divisor data of CY threefolds with $h^{1,1} \leq 6$. We computed the Hodge numbers of prime toric divisors via the methods described in section 2.2 which is largely consistent with the data presented in [3]. We compare the D3-charge contribution of SO(8) stacks (local D7-tadpole cancellation) with that of Whitney branes (non-local D7-tadpole cancellation). We argue that there is an enhancement of about a factor of 5 between local and non-local D7-tadpole cancellation.

Recalling (3.2), it is clear that divisors with $h^{(0,1)}(D) = 0$ lead to the largest Euler characteristic. That is, it seems to be profitable to have O7-planes and D7-branes wrapping divisors with Hodge numbers

$$h^{\bullet}(D) = \left\{1, 0, h^{(0,2)}(D), h^{(1,1)}(D)\right\}, \tag{4.1}$$

for which (3.2) leads to

$$\chi(D) = 2\left(1 + h^{2,0}(D)\right) + h^{1,1}(D). \tag{4.2}$$

JHEP08(2022)050

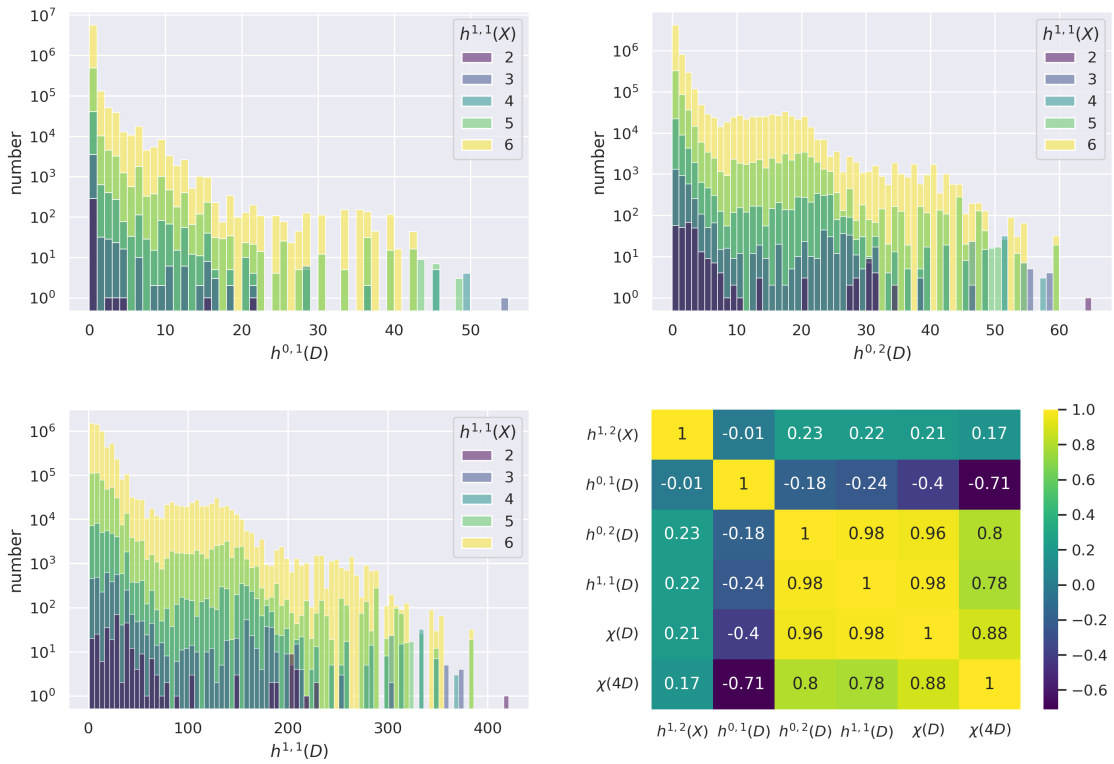

Figure 1. Histogram plots for Hodge numbers $h^{p,q}$ of all divisors at $h^{1,1} \leq 6$. We ignore $h^{0,0}$ given that $h^{0,0}(D) = 1$ for all D. The bottom right plot shows a correlation map for the relevant divisor and CY data.

Clearly, maximising $\chi(D)$ is beneficial from the perspective of the tadpole (3.22). Using the results computed in our database for $h^{1,1} \leq 6$, we compute the Euler characteristic for every divisor finding that the maximal value is[13]

$$\chi(D)\big|_{\max} = 549\,. \tag{4.3}$$

A complete overview of the distribution of both Hodge numbers as well as Euler characteristics of (prime toric) divisors appearing in the KS database up to $h^{1,1} = 6$ is shown in figure 1 and figure 2 respectively.

In figure 2, we show the distribution of Euler numbers for different types of divisors. Clearly, non-rigid divisors result in the largest $\chi(D)$ with the maximum given by (4.3), while $\chi(D_{\text{rigid}})\big|_{\max} = 111$ for rigid divisors. Those divisors D with non-positive $\chi(D)$ are in fact associated with Wilson divisors[14] with $h^{0,1}(D) > 0$ and $h^{0,2}(D) = 0$ out of which 44.67% are Exact-Wilson divisors with $h^{0,1}(D) = 1$.

In figure 1, we present a correlation map for Hodge and Euler numbers of divisors. The correlations between $\chi(D)$ and the corresponding Hodge numbers is clear from (3.2). In our data, there are no significant correlations between any of the variables shown on the

[13]For models that admit exchange involutions, one verifies that $\chi(D)\big|_{\max} = 492$ in agreement with [10].

[14]We compared these results to the Hodge numbers obtained from the database [3] and found overall agreement.

JHEP08(2022)050

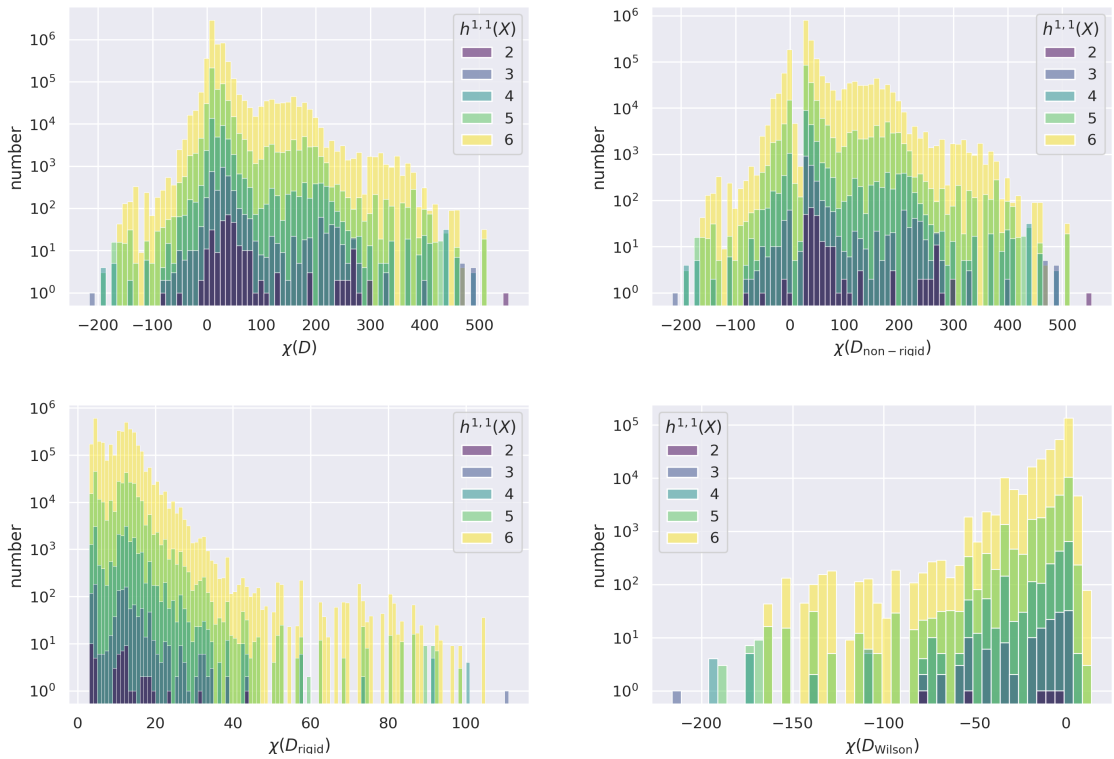

Figure 2. Histogram plots for Euler numbers of divisors. In the first row, we computed the distribution of Euler numbers for all divisors D on the left and for only non-rigid divisors D_{nr} with either $h^{0,1}(D) > 0$ or $h^{0,2}(D) > 0$. The second row shows the Euler characteristic for divisors which are rigid (left) or Wilson (right) with $h^{1,0} \neq 0$, $h^{2,0} = 0$.

bottom right of figure 1 with the number of Kähler moduli $h^{1,1}(X)$ of the CY X nor with $h^{0,0}(D)$ which is why we omitted the later two. Interestingly, we observe that there is an anti-correlation between $h^{0,1}(D)$ with $h^{0,2}(D)$ and $h^{1,1}(D)$, while at the same time $h^{0,2}(D)$ and $h^{1,1}(D)$ are strongly correlated. This implies that there is an obvious trend where larger $h^{1,1}(D)$ implies large $h^{0,2}(D)$ plus small $h^{0,1}(D)$ and, hence, larger $\chi(D)$. We observe similar correlations of $\chi(D)$ and $\chi(4D)$ with $h^{1,2}(X)$ which will be confirmed further below in figure 3.

4.4 D3-charge in the database and non-local D7-tadpole cancellation

In this section, we will study how the D3-tadpole contribution from localised sources varies in the dataset we are taking into account.

We begin by considering only the D3-charge coming from the O-planes. We present an overview of their D3-charge contribution in figure 3. We ignored models with positive $Q_{\text{O}p}^{\text{tot}}$. The colouring indicates the value of $h_+^{1,2}$ where we clearly see the trend expected from (3.4): non-vanishing $h_+^{1,2}$ decreases the absolute value of the D3-charge contribution. The models on the diagonal line have $h_+^{1,2} = 0$ and follow the expected scaling $\sim -h_-^{1,2}/3$ as derived in (3.4).

JHEP08(2022)050

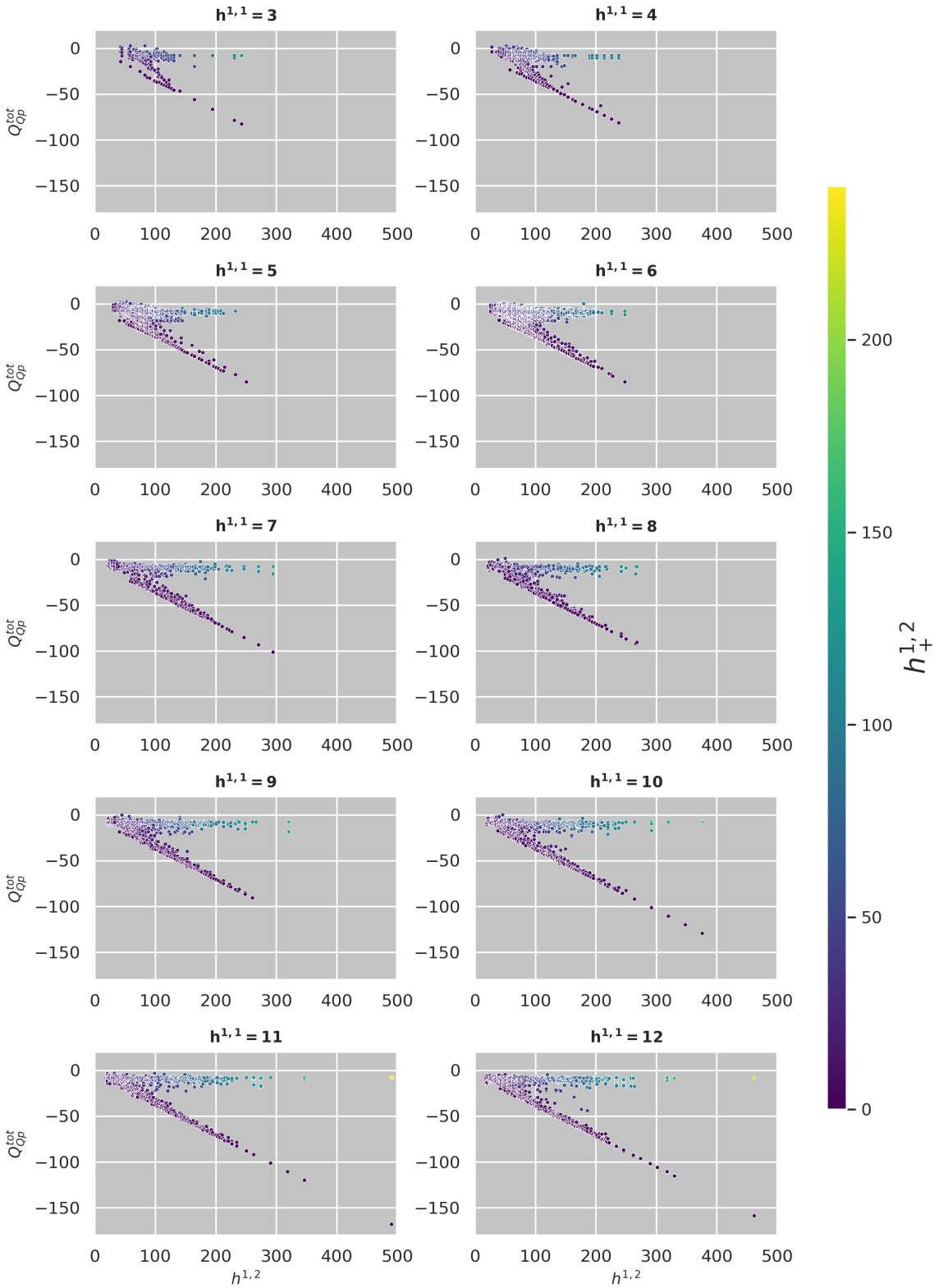

Figure 3. Overview of the D3-charge contribution contributed by Op-planes only. For $h^{1,1} \geq 7$, we present the data for models collected in table 3, while for $h^{1,1} \leq 6$ we use the models of table 2. The maximal absolute value for the D3-charge comes from orientifolds with Hodge numbers $(h^{1,1}, h_-^{1,2}, h_+^{1,2}) = (11, 491, 0)$ where we find $Q_{Op}^{\text{tot}} = -168$.

JHEP08(2022)050

Let us introduce the D7-branes. We analyse the situation in the absence of gauge flux on the D7-branes.[15] For each model (derived from a choice of CY X and involution), we try to cancel the D7-tadpole generated by the O7-planes by a D7-brane configuration that maximizes their (absolute value of the) contribution to the D3-charge. For each O7-plane that we find we then work out the topology of the wrapped divisor. If we have O7-planes on rigid or Wilson divisors, we cancel the D7-tadpole by a SO(8) stacks. For O7-planes on deformation divisors with $h^{0,2}(D) > 1$, we cancel the D7-tadpole non-locally through Whitney branes, see appendix A for details. Finally, whenever $h^{0,2}(D) = 1$, we construct (3.9) explicitly to check for eventual factorisation; if no factorization is forced, we add a Whitney brane.

For each $h^{1,1}(X)$, we pick the model (X and involution) whose localised sources contribute most to the total D3-charge. In table 4, we report the absolute value of the total D3-charge from these localised sources for two cases: 1) the D7-tadpole is canceled by putting $4 + 4$ D7-branes on top of all the O7-planes (local D7-tadpole cancellation) and 2) we put Whitney branes on all non-rigid O7-plane divisors (non-local D7-tadpole cancellation).

Let us stress the difference between local and non-local D7-tadpole cancellation. If we were to simply add (4+4) D7-branes on top of each of the D7-branes to cancel the D7-tadpole locally, this would amount to[16]

$$Q_{\mathrm{D3}} \approx \underbrace{-(4+4)\frac{\chi(D_i)}{24}}_{\mathrm{D7}} \underbrace{-\frac{\chi(D_i)}{6}}_{\mathrm{O7}}\,, \tag{4.4}$$

which leads to the conservative estimate

$$\text{local D7-tadpole cancellation: } |Q_{\mathrm{D3}}| \leq 504\,, \tag{4.5}$$

as one can check in table 4. This is precisely the upper bound obtained in (3.31) for $(h^{1,1}, h^{1,2}) = (11, 491)$. In figure 4, we show that the D3-tadpole is significantly enhanced by considering more generic brane configurations, as we argued in section 3.4. The results in table 4 show that in this case the total D3-charge extraordinarily exceeds the bound (4.5). In particular, as we argue below in section 5, using instead Whitney branes, the total D3-charge is increased by about a factor of 13, obtaining the following bound on localised sources D3-charge:

$$\text{non-local D7-tadpole cancellation: } |Q_{\mathrm{D3}}| \leq 6,664\,. \tag{4.6}$$

The values stated in table 4 give an upper bound on the total D3-charge. For models with multiple O3-planes at the tip of a throat which are suitable for anti-D3 uplift [43], we obtain $|Q_{\mathrm{D3}}| \leq 3592$ with the maximal value realised for orientifolds with Hodge numbers $(h^{1,1}_{+}, h^{1,2}_{-}) = (12, 274)$.

[15] Freed-Witten anomaly cancellation may force some flux to be non-zero; however one can always choose a flux that minimise its contribution to the D3-charge; in this situation our results are good approximations for the total D3-charge coming from localised sources.

[16] We ignore the contribution from O3-planes here. For models with the minimal $Q^{\mathrm{tot}}_{\mathrm{O}p}$ on the diagonal in figure 3, there are actually no O3-planes which justifies the bound given in (4.5).

JHEP08(2022)050

$h^{1,1}$		2	3	4	5	6	7	8	9	10	11	12
D3-charges $\lvert Q_{\mathrm{D3}}\rvert$	local	276	248	244	256	256	304	276	272	388	504	476
	non-local	3,678	3,272	3,212	3,280	3,280	4,000	3,594	3,408	5,036	6,664	6,258
dP_n (ddP_n)	dP_0 (ddP_0)	10 (*)	117 (*)	1,282 (*)	15,346 (*)	172,469 (*)	526 (*)	656 (*)	1,135 (*)	1,049 (*)	1,424 (*)	2,086 (*)
	dP_1 (ddP_1)	5 (3)	159 (47)	2,677 (726)	39,355 (8,880)	514,099 (93,000)	4,994 (59)	8,743 (34)	15,007 (61)	20,346 (35)	28,962 (87)	31,671 (49)
	dP_2 (ddP_2)	0 (0)	6 (0)	438 (0)	10,926 (0)	184,992 (0)	2,822 (0)	6,060 (0)	10,176 (0)	15,104(0)	22,350 (0)	23,178 (0)
	dP_3 (ddP_3)	0 (0)	6 (0)	359 (0)	9,211 (0)	166,494 (0)	2,182 (0)	4,375 (0)	7,004 (0)	10,850 (0)	15,618 (0)	17,495 (0)
	dP_4 (ddP_4)	0 (0)	2 (0)	78 (0)	2,227 (0)	50,821 (0)	1,119 (0)	2,196 (0)	3,894 (0)	5,851 (0)	8,533 (0)	8,613 (0)
	dP_5 (ddP_5)	0 (0)	15 (0)	524 (0)	9,482 (0)	144,966 (0)	1,499 (0)	2,487 (0)	3,808 (0)	5,612 (0)	7,689 (0)	8,226 (0)
	dP_6 (ddP_6)	3 (3)	37 (31)	418 (201)	5,714 (1,214)	81,636 (4,719)	959 (0)	1,611 (0)	2,492 (0)	3,412 (0)	5,569 (20)	5,839 (0)
	dP_7 (ddP_7)	6 (6)	134 (92)	2,060 (939)	26,032 (6,158)	302,879 (38,692)	1,841 (23)	2,686 (12)	4,063 (21)	4,822 (9)	6,735 (0)	6,933 (12)
	dP_8 (ddP_8)	7 (7)	134 (83)	1,806 (584)	22,442 (3,458)	269,626 (24,109)	1,722 (41)	2,356 (82)	3,283 (91)	4,149 (67)	4,872 (21)	4,654 (66)
divisor topologies	rigid	52	1,164	20,339	297,112	3,840,467	34,423	58,138	94,621	126,190	178,320	187,751
	$h^{0,2}=1$	50	924	8,931	86,418	798,972	6,065	8,431	10,555	12,941	15,501	15,550
	$h^{0,2}>1$	181	1,444	11,486	101,911	910,903	7,689	12,121	18,008	22,478	29,611	27,825
	Wilson	5	143	1,884	24,985	292,468	1,983	4,074	6,400	9,037	12,788	15,754

Table 4. Top: minimal D3-charge contributions from Op-planes and the corresponding total for either local or non-local D7-tadpole cancellation. Middle: distribution of dP_n and diagonal ddP_n divisors. $\mathrm{dP}_0 = \mathbb{P}^2$ always appears diagonally for which we write $(*)$. For $h^{1,1} = 7$, we present the data obtained from random runs. Bottom: summary of topologies of toric divisors encountered in the scan. In the second and third row, we distinguish between deformation divisors ($h^{0,1} = 0$) with $h^{0,2} = 1$ and $h^{0,2} > 1$.

JHEP08(2022)050

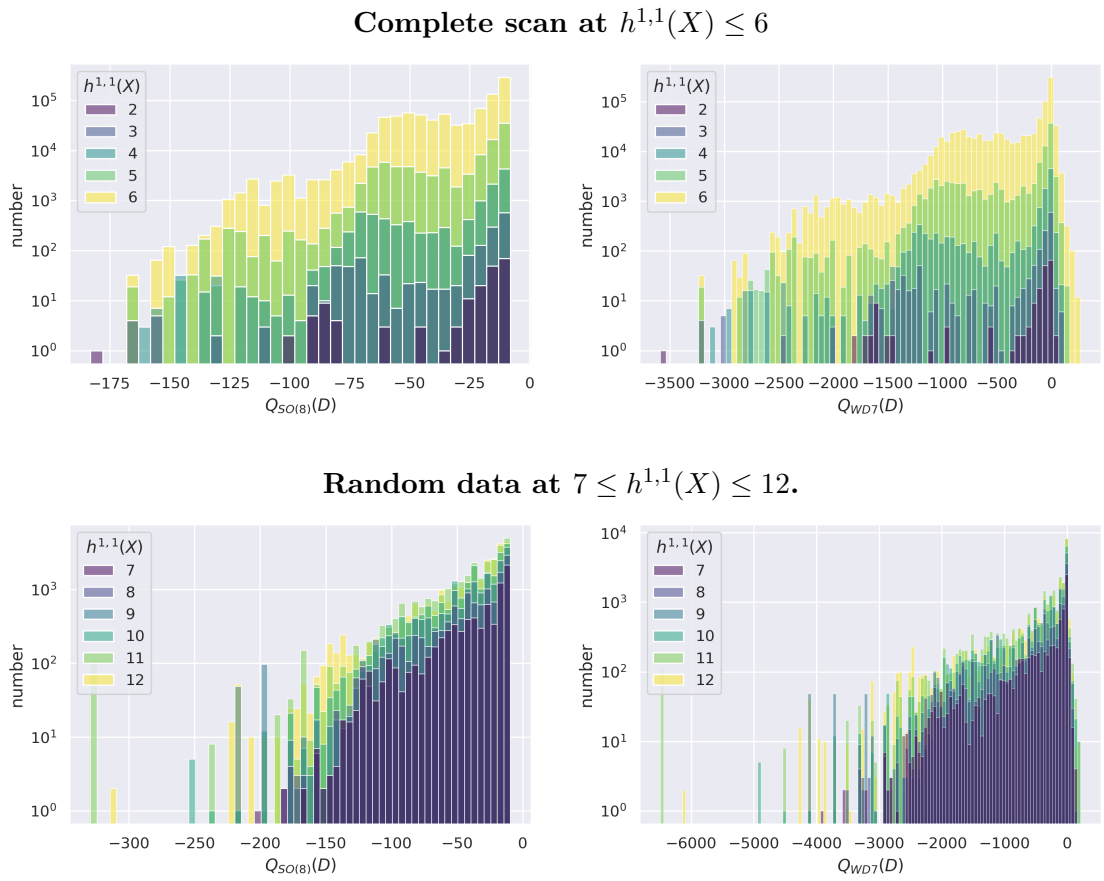

Figure 4. Local vs. non-local tadpole cancellation for data at $h^{1,1}(X) \leq 6$. Left: distribution of $Q_{\mathrm{SO}(8)}(D)$ for divisors with $h^{0,2}(D) > 1$ and $h^{0,1}(D) = 0$. Right: distribution of $Q_{\mathrm{WD7}}(D)$ for the same divisors.

We finally note that we neglected the D3-contribution from fluxes. The fluxes change the total Q_{D3}, both decreasing it (it is the case of a supersymmetric flux, including the flux on the Whitney brane) and increasing it (it is the case of a flux generating a non-zero FI-terms inducing e.g. a T-brane background [45]). These fluxes typically do not change the order of magnitude of our estimations. However they must be taken into consideration in explicit models when computing D3-tadpole cancellation.

Cancelling the tadpole locally through (4+4) D7-branes on top of O7-planes has led to charges $[-72, 8]$ in [5] for CICY orientifolds and $[-60, 0]$ in [3] for toric CY orientifolds with $h^{1,1} \leq 6$ from exchange involutions.[17] In the analysis in [5], it has been shown how non-local tadpole cancellation through generic D7-branes can lead to a significantly larger range $[-264, -24]$. This had consciously been used in many previous applications involving Whitney branes [11, 12, 14, 44], or mild splitting of them [15, 26, 47, 48]

We collect all divisors with Hodge numbers $h^{0,2}(D) > 1$ and $h^{0,1}(D) = 0$ at $h^{1,1}(X) \leq 6$ as computed in [3]. It is then instructive to compare the total D3-charge contribution from

[17] We note that $Q_{\mathrm{D3}} = -2Q^{\mathrm{D3}}_{\mathrm{SO}(8)}$ in the conventions of [5], while $Q_{\mathrm{D3}} = -2Q^{\mathrm{loc}}_{\mathrm{D3}}$ in the convention of [3]. Our convention for the D3-tadpole (3.22) is based on eq. (3.81) in [46] where $Q_{\mathrm{D3}} = 2Q_c$.

JHEP08(2022)050

Complete scan at $h^{1,1} \leq 6$		
$h^{1,1}(X)$	$Q_{\mathrm{SO}(8)}(D)$	$Q_{\mathrm{WD7}}(D)$
2	−25.82	−269.77
3	−28.31	−316.69
4	−29.78	−342.26
5	−30.27	−344.21
6	−30.53	−339.49
7	−30.16	−321.89

Random data at $h^{1,1} \leq 12$		
$h^{1,1}(X)$	$Q_{\mathrm{SO}(8)}(D)$	$Q_{\mathrm{WD7}}(D)$
7	−35.21	−391.76
8	−37.82	−428.97
9	−40.12	−458.18
10	−40.27	−457.08
11	−42.90	−497.89
12	−42.23	−480.87

Table 5. Average D3-charge contribution for local and non-local D7-tadpole cancellation for complete scan (left) and randomise data (right).

a stack of (4+4) D7-branes (local) and Whitney branes (non-local), as shown in figure 4 for $h^{1,1}(X) \leq 6$ and $7 \leq h^{1,1}(X) \leq 12$ respectively, where

$$Q_{\mathrm{SO}(8)}(D) = -(4+4) \cdot \frac{\chi(D)}{24}\,, \qquad Q_{\mathrm{WD7}}(D) \simeq -\frac{\chi(4D)}{12} - 9\int_X D^3\,. \tag{4.7}$$

In the last definition we have neglected the flux contribution (3.29) depending on $F - B_2$, as it does not change the order of magnitude of the Whitney brane D3-charge.

The maximal D3-charge contribution from D7-branes on a single divisor are given by

$$|Q_{\mathrm{SO}(8)}(D)|\,|_{\max} = \begin{cases} 183 & h^{1,1}(X) \leq 6 \\ 329.3 & 7 \leq h^{1,1}(X) \leq 12 \end{cases}\,,$$

$$|Q_{\mathrm{WD7}}(D)|\,|_{\max} = \begin{cases} 3,585 & h^{1,1}(X) \leq 6 \\ 6489.3 & 7 \leq h^{1,1}(X) \leq 12 \end{cases}\,. \tag{4.8}$$

We collected the average D3-charge for both sources in table 5 where $Q_{\mathrm{WD7}}(D)$ is enhanced by a factor of 11 on average.

Large D3-charge and genus-one fibrations. An interesting observation concerns the behaviour of the D3-charge distribution at large $h^{1,2}$. While one discovers no particular structure at small $h^{1,2} < 100$, the regime at large $h^{1,2} > 100$ exhibits, instead of a uniform distribution, two distinct dominant lines. We believe that this emergent structure in the distribution of D3-charges has not yet been observed in the literature.

A hint for what is going on is obtained from previous investigations into the underlying fibration structure of toric CY threefolds at large $h^{1,2}$, see [49–52] and references therein. It is in fact true that CY threefolds in the KS database at sufficiently large Hodge numbers ($h^{1,2}$ larger than 240) are associated with elliptic fibrations over complex base surfaces [49]. At the level of 4D reflexive polytopes Δ°, it is quite straight forward to identify the

JHEP08(2022)050

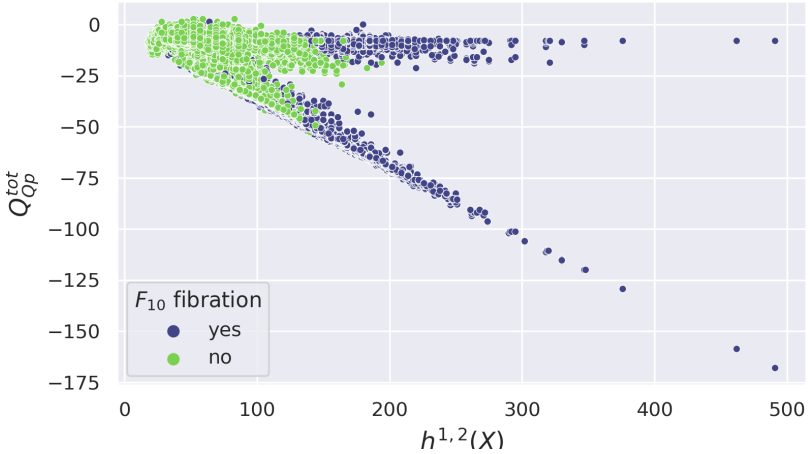

Figure 5. Total D3-charge contributions from O-planes for orientifold models with colours indicating the presence of an underlying $F_{10} = \mathbb{P}[2,3,1]$ fibration.

corresponding fibrations. Namely, whenever Δ° contains a 2D reflexive sub-polytope, the associated CY manifold enjoys a genus one fibration [53].[18] This is indeed a quite common feature: out of the 473.8 million polytopes listed in [1], only 29,223 do not contain any such 2D reflexive polytope [52].[19]

There are only 16 distinct types of genus one fibrations F_i which can be easily identified from the classification of 2D reflexive polytopes.[20] At least at large Hodge numbers, the KS database is dominated by polytopes exhibiting a description of a standard F_{10} fibration [49] (the elliptic fiber is a hypersurface in $\mathbb{P}[2,3,1]$) which therefore also plays a distinguished role in our analysis.

Utilising the algorithm of [52], we computed the 2D reflexive sub-polytopes and the fibration type for each of the favourable 4D polytopes appearing in our analysis, checking that the presence of F_{10} is dominant. We computed the D3-charge distribution for the different types of fibres. In figure 5 we report that the generic elliptic fibre F_{10} dominates especially at $h^{1,2} > 200$ as expected from [49]. Not surprisingly, it is responsible for the universal structure observed in figure 3 independently of $h^{1,1}(X)$. In the regime $h^{1,2} < 200$, similar sub-dominant patterns are found also for elliptic F_6 and F_8 as well as non-elliptic F_4 (the fiber is an hypersurface in $\mathbb{P}^2[2,1,1]$) fibrations. All other fibrations as well as the polytopes without any fibration seem not to experience any enhancement in their D3-charge contribution (i.e. they are mostly constant as functions of $h^{1,2}$) nor are they showing any particularly interesting patterns.

[18] We stress that there are some subtleties occurring when relating the fibration of the polytopes to the actual toric variety, see [52] for a detailed discussion.

[19] In our analysis, we encounter 2,857 (60) of these polytopes in the complete (random) data at $h^{1,1} \leq 7$ ($7 \leq h^{1,1} \leq 12$).

[20] A classification of the 16 distinct polytopes is provided in appendix A of [51] which were previously studied in [54] and play a role in F-theory [50, 55–57].

JHEP08(2022)050

Let us try to explain what happens for the F_{10} case. The CY equation takes the Weierstrass form, i.e.,

$$y^2 = x^3 + f(w)xz^4 + g(w)z^6 \,. \tag{4.9}$$

Here, w denotes collectively coordinates on the toric two-dimensional base B, whereas x, y, z are projective coordinates on $\mathbb{P}[2,3,1]$ with x and y being sections respectively of $\bar{K}_B^{\otimes 2}$ and $\bar{K}_B^{\otimes 3}$. For consistency of the equation, f and g must be sections respectively of $\bar{K}_B^{\otimes 4}$ and $\bar{K}_B^{\otimes 6}$

At fixed w, the equation (4.9) describes a torus. The $\mathbb{Z}_2$ involution of the torus (with four fixed points) is implemented in this algebraic setup by taking $y \mapsto -y$ (or equivalently $z \mapsto -z$). The Weierstrass form is already invariant. Hence, if one takes (4.9) as the defining equation for the CY three-fold, one has the involution that inverts y. This toric coordinate is manifestly of high degree (and among the coordinates of this threefold, y is the highest degree one) and correspondingly the Euler characteristic of D_y is large. This is the main reason why we find the largest D3-charges for these models.

In studying the F_{10} case, we realise another fact: one may add to (4.9) also a term proportional to x^2z^2 and then consider the involution $x \mapsto -x$. x is also high degree and the D3-charge one would obtain from such an involution is still large, even if lower than the one obtained by $y \mapsto -y$. However, there is a pathology: the invariant CY equation would be

$$y^2 = \left(a(w)x^2 + g(w)z^4\right) z^2 \,, \tag{4.10}$$

that has a manifest (non crepantly resolvable) singularity at $z = y = 0$. Since xyz is the SR-ideal, the D7/O7's do not touch the singularity and their topological invariants do not feel the pathology. However, we excluded it from our analysis as Δ_k is not reflexive because the monomial x^3 is associated with a vertex in the full dual polytope Δ. If we had included such models, we would have obtained a second diagonal line in our plots of models with large D3-charge.

5 Example with $(h^{1,1}, h^{1,2}) = (11, 491)$

To be more specific, let us describe in more detail the model with the potentially largest D3-tadpole reported in table 4. It turns out that this model is obtained from an involution of a CY threefold X with Euler characteristic $\chi(X) = -960$ and Hodge numbers $(h^{1,1}, h^{1,2}) = (11, 491)$. The GLSM charges of X are collected in table 6; the SR ideal is given by

$$\begin{aligned} I_{\rm SR} = \{ & z_1z_2, z_3z_6, z_3z_7, z_3z_8, z_3z_9, z_3z_{10}, z_3z_{11}, z_3z_{12}, z_3z_{13}, z_3z_{14}, z_4z_6, z_4z_7, z_4z_8, z_4z_9, \\ & z_4z_{10}, z_4z_{11}, z_4z_{12}, z_4z_{14}, z_5z_6, z_5z_7, z_5z_8, z_5z_9, z_5z_{10}, z_5z_{12}, z_6z_8, z_6z_{10}, z_6z_{12}, z_6z_{13}, \\ & z_6z_{14}, z_6z_{15}, z_7z_{10}, z_7z_{12}, z_7z_{13}, z_7z_{14}, z_7z_{15}, z_8z_{12}, z_8z_{13}, z_8z_{14}, z_8z_{15}, z_9z_{12}, z_9z_{14}, \\ & z_9z_{15}, z_{10}z_{14}, z_{10}z_{15}, z_{11}z_{15}, z_{12}z_{15}, z_4z_5z_{15}, z_5z_{13}z_{14}, z_5z_{13}z_{15}, z_7z_9z_{11}, z_8z_9z_{11}, \\ & z_9z_{10}z_{11}, z_{10}z_{11}z_{13}, z_{11}z_{12}z_{13}, z_{11}z_{13}z_{14} \} \,. \end{aligned} \tag{5.1}$$

The 2nd Chern numbers are:

$$\int_{D_i} c_2(X) = \{24, 24, 168, 368, 548, -4, -4, -4, -4, -4, -4, -4, -4, -4, -4\} \,. \tag{5.2}$$

JHEP08(2022)050

z_1	z_2	z_3	z_4	z_5	z_6	z_7	z_8	z_9	z_{10}	z_{11}	z_{12}	z_{13}	z_{14}	z_{15}	
1	1	12	28	42	0	0	0	0	0	0	0	0	0	0	84
0	0	6	14	21	1	0	0	0	0	0	0	0	0	0	42
0	0	5	12	18	0	1	0	0	0	0	0	0	0	0	36
0	0	4	10	15	0	0	1	0	0	0	0	0	0	0	30
0	0	4	9	14	0	0	0	1	0	0	0	0	0	0	28
0	0	3	8	12	0	0	0	0	1	0	0	0	0	0	24
0	0	3	7	10	0	0	0	0	0	1	0	0	0	0	21
0	0	2	6	9	0	0	0	0	0	0	1	0	0	0	18
0	0	2	4	7	0	0	0	0	0	0	0	1	0	0	14
0	0	1	4	6	0	0	0	0	0	0	0	0	1	0	12
0	0	0	2	3	0	0	0	0	0	0	0	0	0	1	6

Table 6. Weights for the model with $h^{1,1} = 11$ and $h^{1,2} = 491$.

Finally, the Hodge numbers of the divisors can be computed to be:

$$\begin{aligned} h^\bullet(D_1) = h^\bullet(D_2) &= \{1,0,1,20\}\,, & h^\bullet(D_3) &= \{1,0,13,140\}\,, \\ h^\bullet(D_4) &= \{1,0,51,392\}\,, & h^\bullet(D_5) &= \{1,0,118,750\}\,, \\ h^\bullet(D_i) &= \{1,0,0,2\}\,, & i &= 6,\ldots,15\,. \end{aligned} \tag{5.3}$$

Related to the discussion above, one finds that this CY exhibits an F_{10} fibration with coordinates $z_4, z_5, z_{15} = x, y, z$ over the Hirzebruch surface $\mathbb{F}_{12}$ as can be seen from the last line in the GLSM charge matrix in table 6.[21] Our analysis shows that the allowed values of the D3-charge from Op-planes are $8 \leq |Q^{\text{tot}}_{\text{O}p}| \leq 168$. The maximally allowed D3-charge from O7-planes is actually obtained from (recall (3.4) and that all other $D_{i>5}$ are dP$_1$ divisors)

$$\chi(D_5) + \chi(D_{15}) + 4 \cdot \chi(\text{dP}_1) = 2\left(h^{1,2} + h^{1,1} + 2\right) = 1,008\,. \tag{5.4}$$

It is associated with the standard involution of the torus fibre $z_5 \to -z_5$ as argued above.

For this reason, let us study this involution

$$z_5 \to -z_5 \tag{5.5}$$

which gives rise to O7-planes on D_5, D_6, D_8, D_{12}, D_{13} and D_{15} and invariant Hodge numbers $(h^{1,2}_-, h^{1,2}_+) = (491, 0)$. There are no O3-planes. As it can be read from the Hodge

[21] In fact, $h^{1,2} = 491$ is the largest possible value for any elliptic CY threefold [58].

JHEP08(2022)050

numbers (5.3), the Euler characteristic of the O7 divisors are $\chi(D_5) = 988$ and $\chi(D_i) = 4$ for $i = 6, 8, 12, 13, 15$. Hence, The O7-planes contribute to the D3 charge with:

$$Q_{\text{O7}}^{\text{tot}} = -\sum_{k=5,6,8,12,13,15} \frac{\chi(D_k)}{6} = -168\,. \tag{5.6}$$

As concerns the branes configuration, the divisors D_6, D_8, D_{12}, D_{13} and D_{15} are rigid and then support an SO(8) stack.[22] The D7-tadpole from the D_5 divisors will instead be canceled by a Whitney brane.

We choose a B-field that allow to have zero flux on each D7-brane:

$$B_2 = \frac{1}{2}\left(D_6 + D_8 + D_{12} + D_{13} + D_{15}\right)\,. \tag{5.7}$$

Since the divisors $D_{6,8,12,13,15}$ do not intersect each other, the pull-back of the B-field on the divisor D_i is equal to $\iota^*_{D_i} B_2 = \frac{D_i}{2}$ and then it cancels the non-integral flux that is necessary for Freed-Witten anomaly cancellation, leading to $\mathcal{F}_i = 0$. As regarding the Whitney brane, we need to check that there exists an integral 2-form F that cancels either $\frac{3}{2}D_5 + B_2$ or $\frac{3}{2}D_5 - B_2$ in (3.17). This happens, because $D_5 + B_2$ is an even form, as it can be checked from the GLSM weights in table 6.

Taking vanishing fluxes on each D7-brane, the D3-charge contribution is only geometrical. The SO(8) stacks contribute to the D3-charge as

$$Q_{\text{SO(8)}}^{\text{tot}} = -\sum_{i=6,8,12,13,15} \frac{\chi(D_i)}{3} = -5 \cdot \frac{4}{3} = -\frac{20}{3}\,, \tag{5.8}$$

while the main contribution to the D3-charge comes from the Whitney brane, whose geometric contribution (3.28) is

$$Q_{WD7,\text{geom}} = -\frac{\chi(4D_5)}{12} - 9\int_X D_5^3 = -\frac{19,468}{3}\,, \tag{5.9}$$

where we used $\chi(4D_5) = 30,352$ and $D_5^3 = 440$. Cancelling the D7-tadpole from D_5 by a Whitney brane, instead of an SO(8) stack, increases the D3-charge from 7-branes by approximately a factor of

$$\frac{Q_{WD7,\text{geom}}^{D_5}}{Q_{\text{SO(8)}}^{D_5}} \approx 20\,, \tag{5.10}$$

where

$$Q_{\text{SO(8)}}^{D_5} = -\frac{\chi(D_5)}{3} = -\frac{988}{3}\,. \tag{5.11}$$

The total D3-charge contribution from localised sources is then

$$Q_{\text{D3}} = Q_{\text{O7}}^{\text{tot}} + Q_{\text{SO(8)}}^{\text{tot}} + Q_{WD7,\text{geom}} = -6664\,, \tag{5.12}$$

as reported in table 4.

[22] The SO(8) stacks do not intersect each other.

JHEP08(2022)050

To stabilise all the moduli via non-perturbative effects, it would be favourable to have instantons on the other rigid divisors. Since the B-field (5.7) does not allow to have vanishing fluxes $\mathcal{F}_{E3}$ on any of these divisors we cannot have O(1) instantons. On the other side, rank-2 instantons might be allowed [36] provided that one checks that no chiral modes arise at the intersection with the SO(8) stacks. This model is of course not suitable for anti-D3 uplift since there are no O3-planes, but in principle we could engineer a T-brane background that allows for de Sitter minima [45].

6 Conclusions

In this paper, we generated a database of CY orientifolds from holomorphic reflection involutions of CY hypersurfaces. We determined the orientifold configurations for all favourable FRSTs for $h^{1,1} \leq 7$. We found more than 70 million involutions of which over 20 million correspond to smooth compactifications. Singular involutions were identified and their structure deserves further investigation. We also specified the number of cases with either O3 or O7 planes suitable for antibrane or T-brane uplifts.

We plotted several relevant quantities such as the Euler number and Hodge numbers of the divisors and the value of the D3 brane charges. We observed some interesting patterns in the distribution of the models. In particular the values of the D3 charges show non-trivial structures, such as higher concentration of models in some particular directions, that would be interesting to understand from the more mathematical perspective.

Our algorithm is in principle capable of computing orientifolds for any $h^{1,1}$. We provided partial results for triangulations up to $h^{1,1} = 12$. We found several classes of models with different behaviour in their D3-charge and O-plane configuration. Most importantly, we provided evidence for a large class of models for which the D3-charge from Op-planes grows $\sim -(h^{1,1}_{+} + h^{1,2}_{-})/3$, i.e., linearly with the number of invariant geometric moduli. This constitutes an upper bound on the absolute value of the total D3-charge from D7/O7's and O3's.

We further showed that cancelling the D7-tadpole non-locally via Whitney branes as opposed to locally via SO(8) stacks on top of O7-planes increases the overall D3-charge by up to factors of 12. We presented an explicit orientifold with Hodge numbers $(h^{1,1}, h^{1,2}) = (11, 491) = (h^{1,1}_{+}, h^{1,2}_{-})$ which led to a total D3-charge of $|Q_{\mathrm{D3}}| = 6,664$. This value beats previous D3-charge records in type IIB by a large margin (recall table 1). It provides the necessary space to turn on background fluxes which in turn are relevant for stabilising moduli and model building. Beyond that, our database contains a plethora of other models, $357,730$ to be precise, with $|Q_{\mathrm{D3}}| > 504$ making it an excellent starting point for the construction of trustable string vacua. An explicit calculation of moduli stabilisation for these vacua is beyond the scope of this paper.

An important result of this paper concerns the non-trivial D3-charge distribution as a function of $h^{1,2}$. We provided evidence based on the existence of 2D reflexive sub-polytopes that this is mainly a result of special genus one fibrations of the associated CY threefolds, especially elliptic F_{10} (hypersurface in $\mathbb{P}[2,3,1]$) and non-elliptic F_4 (hypersurface in $\mathbb{P}[1,1,2]$) fibrations. The patterns observed in figure 3 are directly linked to reflecting

JHEP08(2022)050

either coordinates along fibre or the base. Further, we put forward an argument for F_{10} fibrations that involutions involving coordinates along the fibre generically maximise the bound on the D3-charge. It would be interesting to further explore the role of genus one fibrations in the context of $\mathcal{N} = 1$ compactifications of type IIB to 4 dimensions.

In the future, it is desirable to extend the database in the regime $h^{1,1} \geq 12$. Recent works [2, 18, 59] demonstrated that triangulations of polytopes with large $h^{1,1}$ can be constructed efficiently. However, exhaustive scans or random sampling might be impractical which is why a more targeted approach by employing optimisation methods would be favourable as previously applied in the search for string vacua [60–67]. In the same spirit, it would also be exciting to relate our database to the one of CICYs [5] and combine it with the one for divisor exchange involutions [3]. For instance, as compared to [3], we have not glued together the Kähler cones of equivalent triangulations. Similar to [5], a large fraction of the orientifolds contained in the database are singular which can in special cases like the conifold be resolved as discussed in [68] for the CICY landscape. Such resolutions might lead to new CY threefolds that are not contained in the KS database.

Acknowledgments

We would like to thank Andres Collinucci, Xin Gao, Arthur Hebecker, Sven Krippendorf, Francesco Muia and Pramod Shukla for useful discussions. AS acknowledges support by the German Academic Scholarship Foundation and by DAMTP through an STFC studentship. The work of FQ has been partially supported by STFC consolidated grants ST/P000681/1, ST/T000694/1. C.C. and R.V. acknowledge support by INFN Iniziativa Specifica ST&FI.

A Examples with Whitney branes

In this appendix, we study two CYs at $h^{1,1} = 3$ which admit divisors of different topologies. For each toric divisor D_i we study a Whitney brane given by the equation

$$\eta_i^2 - z_i^2 \chi_i = 0\,, \tag{A.1}$$

in order to see whether the line bundles $\mathcal{O}(4D_i)$ and $\mathcal{O}(6D_i)$ force the locus (A.1) to factorise.

All in all, our analysis suggests that $h^{0,2}(D) > 1$ always leads to proper Whitney branes, while for divisors with $h^{0,2}(D) = 1$ the factorisation depends on the actual GLSM weight matrix. In any case, we are mostly interested in divisors of maximal Euler number for which generically $h^{0,2}, h^{1,1} \gg 1$.

A.1 Example with an SO(8) stack for a non-rigid SD1 divisor

We consider the model (`POLYID`: 237, `TRIANGN`: 1 in [16]) with weight matrix in table 7 and SR ideal

$$I_{\text{SR}} = \{z_1 z_6, z_2 z_5, z_3 z_4 z_7\}\,. \tag{A.2}$$

JHEP08(2022)050

z_1	z_2	z_3	z_4	z_5	z_6	z_7	D_H
0	0	1	1	1	1	4	8
0	1	0	0	1	1	3	6
1	0	1	0	1	2	5	10

Table 7. Weights for polytope with ID 237 at $h^{1,1} = 3$.

Following the procedure outlined in section 2.2, we computed the Hodge numbers

$$\begin{aligned} &h^\bullet(D_1) = \{1,0,0,9\}\,, && h^\bullet(D_2) = \{1,0,0,8\}\,, && h^\bullet(D_3) = \{1,0,1,21\}\,, \\ &h^\bullet(D_4) = \{1,0,0,12\}\,, && h^\bullet(D_5) = \{1,0,2,29\}\,, && h^\bullet(D_6) = \{1,0,3,38\}\,, \\ &h^\bullet(D_7) = \{1,0,26,177\}\,. \end{aligned} \tag{A.3}$$

We have three rigid divisors D_1, D_2, D_4 with D_1 a dP_8 and D_2 a dP_7, one SD1 divisor D_3 and three non-rigid (deformation) divisors D_5, D_6, D_7.

Let us now study the defining equation (A.1) for D7-brane configurations on each of the divisors. For the rigid divisors D_1, D_2, D_4, the generic section of $\mathcal{O}(4D_i), \mathcal{O}(6D_i)$ are forced to factorise as

$$\eta_i = z_i^4\,, \quad \chi_i = z_i^6\,,\ i \in \{1,2,4\}\,. \tag{A.4}$$

giving an SO(8) stack. In contrast, we have generic polynomials for the non-rigid divisors D_5, D_6, D_7 and hence proper Whitney brane configurations.

The more interesting scenario concerns the SD1 divisor $D_3 = \{z_3 = 0\}$. Looking at the GLSM charges in table 7, the degrees for z_3 are given by $(1,0,1)$ which implies that $z_3 = 0$ can be modified only through combinations of z_1 and z_4 with weights $(0,0,1)$ and $(1,0,0)$ respectively. This is because all other coordinates z_i, $i \neq 1,3,4$, have degrees $(*,1,*)$. Thus, we may equivalently write

$$z_3 + \alpha z_1 z_4 = 0 \tag{A.5}$$

which is the only possible deformation of D_3 and hence $h^{0,2}(D_3) = 1$.

The Whitney brane is a representative of the class $8[D_3]$ with degrees $(8,0,8)$. A generic element of this class is of the form

$$P_8(z_3\,,\, z_1 z_4) \equiv \sum_{i=0}^{8} \alpha_i\, z_3^i\, (z_1 z_4)^{8-i} = 0\,, \tag{A.6}$$

where P_8 is a homogeneous polynomial of degree 8 in two variables. Clearly, the equation $P_8(X,Y) = 0$ admits precisely 8 zeros which allows us to write it as

$$\prod_{i=1}^{4} (z_3 - \beta_i(z_1 z_4))(z_3 + \beta_i(z_1 z_4)) = 0\,, \tag{A.7}$$

JHEP08(2022)050

z_1	z_2	z_3	z_4	z_5	z_6	z_7	D_H
0	0	1	1	1	2	1	6
0	1	0	0	1	1	0	3
1	0	2	3	2	4	0	12

Table 8. Weights for polytope with ID 57 at $h^{1,1} = 3$.

where we also imposed that our representative is an invariant locus under the involution $z_3 \mapsto -z_3$. This generic factorisation is valid for all invariant representatives of $8[D_3]$, hence also for the Whitney brane in this class.

The equation (A.7) tells us that the Whitney brane corresponding to the divisor D_3 is forced to factorise into 4 pairs of brane/image-brane, that need not necessarily be parallel, i.e., they can in principle intersection[23]

Notice that the above argument would fail if there was an additional coordinate z_0 with degrees $(2, 0, 1)$ for which e.g. the class $2[D_3]$ is represented by

$$z_3^2 + z_3 z_1 z_4 + (z_1 z_4)^2 + z_0 z_1 = 0\,. \tag{A.8}$$

The additional monomial $z_0 z_1$ spoils the factorisation of the branes discussed above. We see no reason for why such situations should not be realised in the KS database. Indeed, the next section provides an explicit example with a divisor with $h^{0,2} = 1$ that looks topologically like a K3 divisor, but whose Whitney brane does not factorise.

A.2 Example with a divisor with $h^{p,q} = h^{p,q}(K3)$

We consider the model (`POLYID`: 57, `TRIANGN`: 3 in [16]) with weight matrix in table 8 and SR ideal

$$I_{\text{SR}} = \{z_1 z_4, z_2 z_5, z_3 z_6 z_7\}\,. \tag{A.9}$$

We find that the Hodge numbers for the toric divisors are given by

$$\begin{aligned} &h^\bullet(D_1) = \{1, 0, 0, 10\}\,, && h^\bullet(D_2) = \{1, 0, 0, 8\}\,, && h^\bullet(D_3) = \{1, 0, 1, 20\}\,, \\ &h^\bullet(D_4) = \{1, 0, 2, 30\}\,, && h^\bullet(D_5) = \{1, 0, 2, 28\}\,, && h^\bullet(D_6) = \{1, 0, 6, 56\}\,, \\ &h^\bullet(D_7) = \{1, 1, 0, 2\}\,. \end{aligned} \tag{A.10}$$

We have two rigid divisors D_1, D_2 with D_2 a dP_7, one Wilson divisor D_7, one SD2 divisor D_4 and two additional non-rigid (deformation) divisors D_5, D_6. The last divisor D_3 looks topologically like a K3 surface. Below we argue why it is not actually the case.

For the rigid divisors D_1, D_2 and the Wilson divisor D_7, we have SO(8) stacks. For the non-rigid divisors D_4, D_5, D_6, we have generic polynomials and hence proper Whitney brane configurations.

[23]For K3 divisors, we expect to find similar situations where the D7-branes are however expected to be parallel without any intersection.

JHEP08(2022)050

For the would-be K3 divisor D_3, a closer inspection of the weight system in table 8 shows that the equation $z_3 = 0$ can be deformed such that

$$z_3 + \alpha z_1^2 z_7 = 0 \tag{A.11}$$

and, given that this is the only possible deformation, $h^{0,2}(D_3) = 1$. On the other hand, the class $2[D_3]$ may be represented by

$$z_3^2 + \alpha_1 z_3 z_1^2 z_7 + \alpha_2 \left(z_1^2 z_7\right)^2 + \beta z_1 z_4 z_7 = 0\,. \tag{A.12}$$

This implies that $z_3^8 = 0$ can be modified in such a way that

$$\sum_{i=0}^{8}\sum_{j=0}^{4} \alpha_{ij} z_3^{8-i-2j} \left(z_1^2 z_7\right)^i (z_1 z_4 z_7)^j = 0\,. \tag{A.13}$$

This is a non-homogeneous polynomial in the three coordinates z_3, $z_1^2 z_7$ and $z_1 z_4 z_7$. In particular, it does not factorise which suggests that we obtain a fully recombined D7-brane in the class $8[D_3]$.

We now argue that the above obstruction to the factorisation of the Whitney brane appears because D_3 is not a K3 surface. In fact, a K3 surface has trivial first Chern class $c_1(K3)$. If it is embedded as a divisor S into a CY threefold, $c_1(S) = -\iota_S^* S$, then

$$\iota_S^* S = 0 \qquad \Rightarrow \qquad \int_X S \wedge S \wedge D = 0 \;\; \forall D \in H^{1,1}(X) \tag{A.14}$$

The Hodge numbers are basically determined (when $h^{1,0} = 0$) by the Euler characteristic and arithmetic genus of S, that only depend on (see (2.9), (2.10)) $\int_X S^3$ and $\int_X S^2 \cdot c_2(X)$.

In our example, $\int_X D_3^3 = 0$ and $\int_X D_3^2 c_2(X) = 24$ (and $h^{1,0}(D_3) = 0$), hence giving the Hodge numbers of a K3. However,

$$\int_X D_3 \wedge D_3 \wedge D_i = k_{33i} = 2\,, \qquad i = 2, 5, 6\,. \tag{A.15}$$

The above situation seems to be quite generic and happens for several other examples such as in the polytopes (triangulations) with IDs 193 (3), 60 (1), 205 (6), 247 (2) and 57 (2) in the database of [16].

B Simple example of CY with genus one fibrations: $\mathbb{P}[1,1,1,6,9]$

Let us show an established example with a fibration, namely the degree 18 hypersurface in $\mathbb{P}[1,1,1,6,9]$ [69–71] which is also prominently featured in the LVS [32]. It corresponds to an elliptic fibration over $\mathbb{P}^2$ with fibres F_{10} (hypersurface in $\mathbb{P}[2,3,1]$) and weights summarised in table 9. The SR-ideal reads

$$I_{\rm SR} = \{z_1 z_2 z_3, z_4 z_5 z_6\} \tag{B.1}$$

JHEP08(2022)050

z_1	z_2	z_3	z_4	z_5	z_6	D_H
1	1	1	6	9	0	18
0	0	0	2	3	1	6

Table 9. Weights for $\mathbb{P}[1,1,1,6,9]$.

and the topology of divisors is

$$h^\bullet(D_i) = \{1,0,2,30\}\,, \qquad \chi(D_i) = 36\,, \qquad i = 1,2,3\,, \tag{B.2}$$
$$h^\bullet(D_4) = \{1,0,28,218\}\,, \qquad \chi(D_4) = 276\,, \tag{B.3}$$
$$h^\bullet(D_5) = \{1,0,65,417\}\,, \qquad \chi(D_5) = 549\,, \tag{B.4}$$
$$h^\bullet(D_6) = \{1,0,0,1\}\,, \qquad \chi(D_6) = 3\,. \tag{B.5}$$

This CY threefold X_3 has Hodge numbers $(h^{1,1}, h^{1,2}) = (2, 272)$ and Euler characteristic $\chi(X) = -540$. The most general CY equation with degrees D_H in table 9 reads

$$\begin{aligned} z_5^2 = z_4^3 &+ h_9(z_1,z_2,z_3)\, z_5 z_6^3 + h_{12}(z_1,z_2,z_3) z_4 z_6^4 + h_{18}(z_1,z_2,z_3) z_6^6 \\ &+ h_3(z_1,z_2,z_3) z_4 z_5 z_6 + h_6(z_1,z_2,z_3) z_4^2 z_6^2\,, \end{aligned} \tag{B.6}$$

that, by a coordinate change can be brought in a Weierstrass form. Let us denote the $\mathbb{P}^2$ base of X_3 as B and the associated canonical class as K_B. Then h_{3n} are sections of $\mathcal{O}(-nK_B)$.

In the notation of [69], we may write $D_6 = H - 3L$ where $D_4 = 2H$, $D_5 = 3H$ and $D_i = L$, $i = 1,2,3$. The intersection pattern is

$$L^3 = 0\,, \qquad L^2 H = 1\,, \qquad L\,H^2 = 3\,, \qquad H^3 = 9\,. \tag{B.7}$$

From $c_2(X_3)\cdot L = 36$ and $c_2(X_3)\cdot H = 102$ we compute

$$\chi(L) = 36\,, \qquad \chi(H) = 111\,, \qquad \chi(H-3L) = \chi(H) - \chi(3L)\,. \tag{B.8}$$

This example is a good arena to understand the emergence of the three lines persisting at large $h^{1,2} > 100$ independently of $h^{1,1}$ as shown in figure 3. The orientifolds obtained from reflection involutions of one of the coordinates z_i, $i = 1,\ldots,6$, fall precisely in three categories. A simple analysis shows that the O-plane configurations are given by:

- $z_i \to -z_i$, $i = 1,2,3$: a single O7-plane wrapping D_i, one O3-plane at $z_j = z_k = z_6 = 0$ and three coinciding O3-planes at $z_j = z_k = z_5 = 0$ where $(i,j,k) \in \{(1,2,3),(2,3,1),(3,1,2)\}$. The Hodge numbers are $(h^{1,2}_+, h^{1,2}_-) = (128, 144)$.
- $z_4 \to -z_4$: a single O7-plane wrapping D_4 and Hodge numbers $(h^{1,2}_+, h^{1,2}_-) = (69, 203)$.
- $z_i \to -z_i$, $i = 5,6$: two O7-planes wrapping both D_5, D_6 and Hodge numbers $(h^{1,2}_+, h^{1,2}_-) = (0, 272)$.

JHEP08(2022)050

The D3-charges from Op-planes are computed as

$$Q_{\mathrm{O}p}^{\mathrm{tot}} = \begin{cases} -8 & \text{reflecting } z_1, z_2, z_3\,, \\ -46 & \text{reflecting } z_4\,, \\ -92 & \text{reflecting } z_5, z_6\,. \end{cases} \tag{B.9}$$

Reflecting along the base $\mathbb{P}^2$ described by $\{z_1, z_2, z_3\}$ gives the minimal D3-charge contribution. The $\mathbb{P}[2,3,1]$-fibre is parametrised by $\{z_4, z_5, z_6\}$ for which we distinguish two cases:

1. If we reflect $z_5 \to -z_5$ (or equivalently $z_6 \to -z_6$), we get four fixed point in the fiber: fibering these points over the base B one obtains the two divisors D_5 and D_6, that will be wrapped by O7-planes. Given that $z_5 \in \mathcal{O}(3H)$, the corresponding O7-plane/D7-brane setup provides the largest contribution to the D3-charge.

2. Let us now consider the involution $z_4 \to -z_4$: the fiber is invariant under it only when it degenerates to

$$z_5^2 = z_6^2 \left(a z_4^2 + b z_6^4 \right)\,. \tag{B.10}$$

   Unfortunately this singularity is inherited by the CY. Ignoring such a singularity, one may conclude that there is an O7-plane wrapping D_4, that does not touch the singularity because of the SR ideal.

Open Access. This article is distributed under the terms of the Creative Commons Attribution License (CC-BY 4.0), which permits any use, distribution and reproduction in any medium, provided the original author(s) and source are credited. SCOAP^3 supports the goals of the International Year of Basic Sciences for Sustainable Development.

References

[1] M. Kreuzer and H. Skarke, *Complete classification of reflexive polyhedra in four-dimensions*, *Adv. Theor. Math. Phys.* **4** (2000) 1209 [hep-th/0002240] [INSPIRE].

[2] M. Demirtas, L. McAllister and A. Rios-Tascon, *Bounding the Kreuzer-Skarke Landscape*, *Fortsch. Phys.* **68** (2020) 2000086 [arXiv:2008.01730] [INSPIRE].

[3] R. Altman, J. Carifio, X. Gao and B.D. Nelson, *Orientifold Calabi-Yau threefolds with divisor involutions and string landscape*, *JHEP* **03** (2022) 087 [arXiv:2111.03078] [INSPIRE].

[4] X. Gao and H. Zou, *Applying machine learning to the Calabi-Yau orientifolds with string vacua*, *Phys. Rev. D* **105** (2022) 046017 [arXiv:2112.04950] [INSPIRE].

[5] F. Carta, J. Moritz and A. Westphal, *A landscape of orientifold vacua*, *JHEP* **05** (2020) 107 [arXiv:2003.04902] [INSPIRE].

[6] K. Dasgupta, G. Rajesh and S. Sethi, *M theory, orientifolds and G-flux*, *JHEP* **08** (1999) 023 [hep-th/9908088] [INSPIRE].

[7] S.B. Giddings, S. Kachru and J. Polchinski, *Hierarchies from fluxes in string compactifications*, *Phys. Rev. D* **66** (2002) 106006 [hep-th/0105097] [INSPIRE].

JHEP08(2022)050

[8] I. Bena, J. Blåbäck, M. Graña and S. Lüst, *The tadpole problem*, *JHEP* **11** (2021) 223 [arXiv:2010.10519] [INSPIRE].

[9] A.P. Braun and R. Valandro, *G_4 flux, algebraic cycles and complex structure moduli stabilization*, *JHEP* **01** (2021) 207 [arXiv:2009.11873] [INSPIRE].

[10] X. Gao, A. Hebecker, S. Schreyer and G. Venken, *The LVS parametric tadpole constraint*, *JHEP* **07** (2022) 056 [arXiv:2202.04087] [INSPIRE].

[11] A. Collinucci, F. Denef and M. Esole, *D-brane Deconstructions in IIB Orientifolds*, *JHEP* **02** (2009) 005 [arXiv:0805.1573] [INSPIRE].

[12] A. Collinucci, M. Kreuzer, C. Mayrhofer and N.-O. Walliser, *Four-modulus 'Swiss Cheese' chiral models*, *JHEP* **07** (2009) 074 [arXiv:0811.4599] [INSPIRE].

[13] C. Crinò, F. Quevedo, A. Schachner and R. Valandro, *De Sitter and D3-tadpole*, work in progress.

[14] M. Cicoli, C. Mayrhofer and R. Valandro, *Moduli Stabilisation for Chiral Global Models*, *JHEP* **02** (2012) 062 [arXiv:1110.3333] [INSPIRE].

[15] M. Cicoli, I.G. Etxebarria, F. Quevedo, A. Schachner, P. Shukla and R. Valandro, *The Standard Model quiver in de Sitter string compactifications*, *JHEP* **08** (2021) 109 [arXiv:2106.11964] [INSPIRE].

[16] R. Altman, J. Gray, Y.-H. He, V. Jejjala and B.D. Nelson, *A Calabi-Yau Database: Threefolds Constructed from the Kreuzer-Skarke List*, *JHEP* **02** (2015) 158 [arXiv:1411.1418] [INSPIRE].

[17] A.P. Braun, C. Long, L. McAllister, M. Stillman and B. Sung, *The Hodge Numbers of Divisors of Calabi-Yau Threefold Hypersurfaces*, arXiv:1712.04946 [INSPIRE].

[18] M. Demirtas, C. Long, L. McAllister and M. Stillman, *The Kreuzer-Skarke Axiverse*, *JHEP* **04** (2020) 138 [arXiv:1808.01282] [INSPIRE].

[19] V.V. Batyrev, *Dual polyhedra and mirror symmetry for Calabi-Yau hypersurfaces in toric varieties*, *J. Alg. Geom.* **3** (1994) 493 [alg-geom/9310003] [INSPIRE].

[20] R. Altman, Y.-H. He, V. Jejjala and B.D. Nelson, *New large volume Calabi-Yau threefolds*, *Phys. Rev. D* **97** (2018) 046003 [arXiv:1706.09070] [INSPIRE].

[21] M. Demirtas, M. Kim, L. McAllister, J. Moritz and A. Rios-Tascon, *Small cosmological constants in string theory*, *JHEP* **12** (2021) 136 [arXiv:2107.09064] [INSPIRE].

[22] M. Demirtas, M. Kim, L. McAllister, J. Moritz and A. Rios-Tascon, *Exponentially Small Cosmological Constant in String Theory*, *Phys. Rev. Lett.* **128** (2022) 011602 [arXiv:2107.09065] [INSPIRE].

[23] V.M. Mehta, M. Demirtas, C. Long, D.J.E. Marsh, L. McAllister and M.J. Stott, *Superradiance in string theory*, *JCAP* **07** (2021) 033 [arXiv:2103.06812] [INSPIRE].

[24] M. Demirtas, N. Gendler, C. Long, L. McAllister and J. Moritz, *PQ Axiverse*, arXiv:2112.04503 [INSPIRE].

[25] J. De Loera, J. Rambau and F. Santos, *Triangulations, Algorithms and Computation in Mathematics*, Springer-Verlag Berlin, Germany (2010) [DOI].

[26] A.P. Braun, M. Rummel, Y. Sumitomo and R. Valandro, *de Sitter vacua from a D-term generated racetrack potential in hypersurface Calabi-Yau compactifications*, *JHEP* **12** (2015) 033 [arXiv:1509.06918] [INSPIRE].

JHEP08(2022)050

[27] R. Blumenhagen, B. Jurke, T. Rahn and H. Roschy, *Cohomology of Line Bundles: a Computational Algorithm*, *J. Math. Phys.* **51** (2010) 103525 [arXiv:1003.5217] [INSPIRE].

[28] R. Blumenhagen, B. Jurke and T. Rahn, *Computational Tools for Cohomology of Toric Varieties*, *Adv. High Energy Phys.* **2011** (2011) 152749 [arXiv:1104.1187] [INSPIRE].

[29] V.I. Danilov and A.G. Khovanskiĭ, *Newton Polyhedra and an Algorithm for Computing Hodge-Deligne Numbers*, *Math. USSR Izv.* **29** (1987) 279.

[30] The Sage Developers, *SageMath, the Sage Mathematics Software System (Version 9.5)*, (2022).

[31] M. Cicoli, D. Ciupke, C. Mayrhofer and P. Shukla, *A Geometrical Upper Bound on the Inflaton Range*, *JHEP* **05** (2018) 001 [arXiv:1801.05434] [INSPIRE].

[32] V. Balasubramanian, P. Berglund, J.P. Conlon and F. Quevedo, *Systematics of moduli stabilisation in Calabi-Yau flux compactifications*, *JHEP* **03** (2005) 007 [hep-th/0502058] [INSPIRE].

[33] J.P. Conlon, F. Quevedo and K. Suruliz, *Large-volume flux compactifications: moduli spectrum and D3/D7 soft supersymmetry breaking*, *JHEP* **08** (2005) 007 [hep-th/0505076] [INSPIRE].

[34] A.P. Braun, A. Hebecker and H. Triendl, *D7-Brane Motion from M-theory Cycles and Obstructions in the Weak Coupling Limit*, *Nucl. Phys. B* **800** (2008) 298 [arXiv:0801.2163] [INSPIRE].

[35] D.S. Freed and E. Witten, *Anomalies in string theory with D-branes*, *Asian J. Math.* **3** (1999) 819 [hep-th/9907189] [INSPIRE].

[36] P. Berglund and I. Garcia-Etxebarria, *D-brane instantons on non-Spin cycles*, *JHEP* **01** (2013) 056 [arXiv:1210.1221] [INSPIRE].

[37] A. Collinucci and R. Savelli, *T-branes as branes within branes*, *JHEP* **09** (2015) 161 [arXiv:1410.4178] [INSPIRE].

[38] A.P. Braun, A. Collinucci and R. Valandro, *G-flux in F-theory and algebraic cycles*, *Nucl. Phys. B* **856** (2012) 129 [arXiv:1107.5337] [INSPIRE].

[39] D.R. Morrison and W. Taylor, *Classifying bases for 6D F-theory models*, *Central Eur. J. Phys.* **10** (2012) 1072 [arXiv:1201.1943] [INSPIRE].

[40] D.R. Morrison and W. Taylor, *Non-Higgsable clusters for 4D F-theory models*, *JHEP* **05** (2015) 080 [arXiv:1412.6112] [INSPIRE].

[41] T.W. Grimm and T. Weigand, *On Abelian Gauge Symmetries and Proton Decay in Global F-theory GUTs*, *Phys. Rev. D* **82** (2010) 086009 [arXiv:1006.0226] [INSPIRE].

[42] R. Kallosh, F. Quevedo and A.M. Uranga, *String Theory Realizations of the Nilpotent Goldstino*, *JHEP* **12** (2015) 039 [arXiv:1507.07556] [INSPIRE].

[43] I. García-Etxebarria, F. Quevedo and R. Valandro, *Global String Embeddings for the Nilpotent Goldstino*, *JHEP* **02** (2016) 148 [arXiv:1512.06926] [INSPIRE].

[44] C. Crinò, F. Quevedo and R. Valandro, *On de Sitter String Vacua from Anti-D3-branes in the Large Volume Scenario*, *JHEP* **03** (2021) 258 [arXiv:2010.15903] [INSPIRE].

[45] M. Cicoli, F. Quevedo and R. Valandro, *de Sitter from T-branes*, *JHEP* **03** (2016) 141 [arXiv:1512.04558] [INSPIRE].

[46] F. Denef, *Les Houches Lectures on Constructing String Vacua*, *Les Houches* **87** (2008) 483 [arXiv:0803.1194] [INSPIRE].

JHEP08(2022)050

[47] J. Louis, M. Rummel, R. Valandro and A. Westphal, *Building an explicit de Sitter*, *JHEP* **10** (2012) 163 [arXiv:1208.3208] [INSPIRE].

[48] M. Cicoli, I. Garcìa-Etxebarria, C. Mayrhofer, F. Quevedo, P. Shukla and R. Valandro, *Global Orientifolded Quivers with Inflation*, *JHEP* **11** (2017) 134 [arXiv:1706.06128] [INSPIRE].

[49] Y.-C. Huang and W. Taylor, *Comparing elliptic and toric hypersurface Calabi-Yau threefolds at large Hodge numbers*, *JHEP* **02** (2019) 087 [arXiv:1805.05907] [INSPIRE].

[50] Y.-C. Huang and W. Taylor, *On the prevalence of elliptic and genus one fibrations among toric hypersurface Calabi-Yau threefolds*, *JHEP* **03** (2019) 014 [arXiv:1809.05160] [INSPIRE].

[51] Y.-C. Huang and W. Taylor, *Mirror symmetry and elliptic Calabi-Yau manifolds*, *JHEP* **04** (2019) 083 [arXiv:1811.04947] [INSPIRE].

[52] Y.-C. Huang and W. Taylor, *Fibration structure in toric hypersurface Calabi-Yau threefolds*, *JHEP* **03** (2020) 172 [arXiv:1907.09482] [INSPIRE].

[53] M. Kreuzer and H. Skarke, *Calabi-Yau four folds and toric fibrations*, *J. Geom. Phys.* **26** (1998) 272 [hep-th/9701175] [INSPIRE].

[54] V. Bouchard and H. Skarke, *Affine Kac-Moody algebras, CHL strings and the classification of tops*, *Adv. Theor. Math. Phys.* **7** (2003) 205 [hep-th/0303218] [INSPIRE].

[55] V. Braun, *Toric Elliptic Fibrations and F-theory Compactifications*, *JHEP* **01** (2013) 016 [arXiv:1110.4883] [INSPIRE].

[56] V. Braun, T.W. Grimm and J. Keitel, *Geometric Engineering in Toric F-theory and GUTs with* U(1) *Gauge Factors*, *JHEP* **12** (2013) 069 [arXiv:1306.0577] [INSPIRE].

[57] D. Klevers, D.K. Mayorga Pena, P.-K. Oehlmann, H. Piragua and J. Reuter, *F-Theory on all Toric Hypersurface Fibrations and its Higgs Branches*, *JHEP* **01** (2015) 142 [arXiv:1408.4808] [INSPIRE].

[58] W. Taylor, *On the Hodge structure of elliptically fibered Calabi-Yau threefolds*, *JHEP* **08** (2012) 032 [arXiv:1205.0952] [INSPIRE].

[59] C. Long, L. McAllister and P. McGuirk, *Heavy Tails in Calabi-Yau Moduli Spaces*, *JHEP* **10** (2014) 187 [arXiv:1407.0709] [INSPIRE].

[60] J. Blåbäck, U. Danielsson and G. Dibitetto, *Fully stable dS vacua from generalised fluxes*, *JHEP* **08** (2013) 054 [arXiv:1301.7073] [INSPIRE].

[61] J. Blåbäck, U. Danielsson and G. Dibitetto, *Accelerated Universes from type IIA Compactifications*, *JCAP* **03** (2014) 003 [arXiv:1310.8300] [INSPIRE].

[62] S. Abel and J. Rizos, *Genetic Algorithms and the Search for Viable String Vacua*, *JHEP* **08** (2014) 010 [arXiv:1404.7359] [INSPIRE].

[63] A. Cole, A. Schachner and G. Shiu, *Searching the Landscape of Flux Vacua with Genetic Algorithms*, *JHEP* **11** (2019) 045 [arXiv:1907.10072] [INSPIRE].

[64] M. Larfors and R. Schneider, *Explore and Exploit with Heterotic Line Bundle Models*, *Fortsch. Phys.* **68** (2020) 2000034 [arXiv:2003.04817] [INSPIRE].

[65] S. AbdusSalam, S. Abel, M. Cicoli, F. Quevedo and P. Shukla, *A systematic approach to Kähler moduli stabilisation*, *JHEP* **08** (2020) 047 [arXiv:2005.11329] [INSPIRE].

[66] I. Bena, J. Blåbäck, M. Graña and S. Lüst, *Algorithmically Solving the Tadpole Problem*, *Adv. Appl. Clifford Algebras* **32** (2022) 7 [arXiv:2103.03250] [INSPIRE].

JHEP08(2022)050

[67] S. Krippendorf, R. Kroepsch and M. Syvaeri, *Revealing systematics in phenomenologically viable flux vacua with reinforcement learning*, arXiv:2107.04039 [INSPIRE].

[68] F. Carta, A. Mininno, N. Righi and A. Westphal, *Thraxions: Towards full string models*, *JHEP* **01** (2022) 082 [arXiv:2110.02963] [INSPIRE].

[69] P. Candelas, A. Font, S.H. Katz and D.R. Morrison, *Mirror symmetry for two parameter models. 2*, *Nucl. Phys. B* **429** (1994) 626 [hep-th/9403187] [INSPIRE].

[70] D.-E. Diaconescu and C. Romelsberger, *D-branes and bundles on elliptic fibrations*, *Nucl. Phys. B* **574** (2000) 245 [hep-th/9910172] [INSPIRE].

[71] F. Denef, M.R. Douglas and B. Florea, *Building a better racetrack*, *JHEP* **06** (2004) 034 [hep-th/0404257] [INSPIRE].

JHEP08(2022)050